

PAGE: Prototype-Based Model-Level Explanations for Graph Neural Networks

Yong-Min Shin, *Student Member, IEEE*, Sun-Woo Kim,
and Won-Yong Shin, *Senior Member, IEEE*

Abstract—Aside from graph neural networks (GNNs) catching significant attention as a powerful framework revolutionizing graph representation learning, there has been an increasing demand for explaining GNN models. Although various explanation methods for GNNs have been developed, most studies have focused on *instance-level* explanations, which produce explanations tailored to a given graph instance. In our study, we propose *Prototype-based GNN-Explainer (PAGE)*, a novel *model-level* GNN explanation method that explains what the underlying GNN model has learned for graph classification by discovering human-interpretable *prototype graphs*. Our method produces explanations for a given *class*, thus being capable of offering more concise and comprehensive explanations than those of instance-level explanations. First, PAGE selects embeddings of class-discriminative input graphs on the graph-level embedding space after clustering them. Then, PAGE discovers a common subgraph pattern by iteratively searching for high matching node tuples using node-level embeddings via a *prototype scoring* function, thereby yielding a prototype graph as our explanation. Using five graph classification datasets, we demonstrate that PAGE qualitatively and quantitatively outperforms the state-of-the-art model-level explanation method. We also carry out experimental studies systematically by showing the relationship between PAGE and instance-level explanation methods, the robustness of PAGE to input data scarce environments, and the computational efficiency of the proposed prototype scoring function in PAGE.

Index Terms—Embedding, model-level explanation, graph classification, graph neural network (GNN), prototype graph

1 INTRODUCTION

1.1 Background and Motivation

GRAPHS are a ubiquitous way to organize a diverse set of complex real-world data such as social networks and molecular structures. Graph neural networks (GNNs) have been widely studied as a powerful means to extract useful features from underlying graphs while performing various downstream graph-related tasks [1]. GNNs are known to have high expressive capability via message passing in effectively learning representations of both nodes and graphs [2], while adopting neural networks as a basic building block to learn the graph structure and node features (attributes).

Despite their strengths, such GNN models lack transparency since they do not offer any human-interpretable explanations of GNN’s predictions for a variety of downstream tasks. Thus, fostering *explainability* for GNN models has become of recent interest as it enables a thorough understanding of the model’s behavior as well as trust and transparency [3], [4]. Recent attempts to explain GNN models mostly highlight a subgraph structure within a given

input graph that contributed most towards the underlying GNN model’s prediction [5], [6], [7], [8], [9], [10], [11], [12], [13], [14], [15]. These so-called *instance-level* explanation methods for GNNs provide an in-depth analysis given a graph instance [16].

Nevertheless, instance-level GNN explanations do not reveal the *general* behavior of the underlying model that has already been trained over the whole dataset, consisting of numerous graphs. In some real-world scenarios, explanations that showcase the decision-making process of GNN models are indeed beneficial. For example, when a black-box GNN model is employed in real-world settings, it is likely that the model will encounter various instances not seen during training. In such a case, understanding a rather general decision-making process of the GNN model will help to anticipate the GNN’s behavior in new environments. This motivates us to study *model-level* explanations that aim to interpret GNNs at the model-level.

Fig. 1 visualizes how instance-level explanation methods differ from model-level explanation methods in order to grasp the general behavior of the pre-trained GNN model. Each graph instance is fed into an instance-level explanation method; thus, to understand the model on the whole dataset, we need further steps such as extraction of common patterns among explanations at the instance-level and aggregation of the extracted patterns [17], [18]. However, model-level explanation methods directly capture how the pre-trained GNN model behaves by presenting what it has learned from the whole dataset; such general behavior is summarized as a form of a human-interpretable subgraph.

To the best of our knowledge, XGNN [17] is the only model-level explanation method for GNN models, which

- Y.-M. Shin is with the School of Mathematics and Computing (Computational Science and Engineering), Yonsei University, Seoul 03722, Republic of Korea. E-mail: jordan3414@yonsei.ac.kr.
- S.-W. Kim was with the Department of Statistics, Yonsei University, Seoul 03722, Republic of Korea. He is now with the Kim Jaechul Graduate School of AI at Korea Advanced Institute of Science and Technology, Seoul 02455, Republic of Korea. E-mail: kswoo97@kaist.ac.kr.
- W.-Y. Shin is with the School of Mathematics and Computing (Computational Science and Engineering), Yonsei University, Seoul 03722, Republic of Korea, and also with Pohang University of Science and Technology (POSTECH) (Artificial Intelligence), Pohang 37673, Republic of Korea. E-mail: wy.shin@yonsei.ac.kr.
(Corresponding author: Won-Yong Shin.)

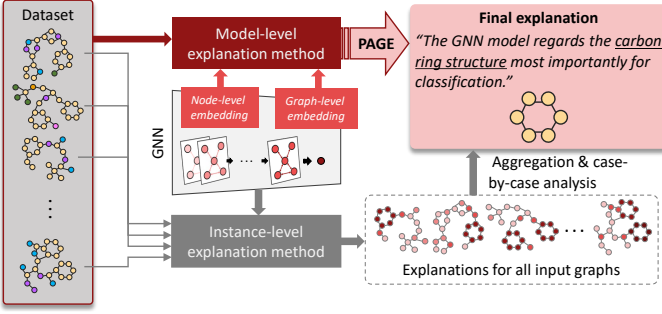


Fig. 1: A comparison between instance-level and model-level explanation methods to capture the general behavior of GNNs.

adopts reinforcement learning as its explanation framework. Since XGNN requires domain-specific knowledge to manually design the reward function, it often fails to produce reliable explanations unless precise rewards are provided according to different types of datasets. Even with plenty of practical challenges, designing model-level explanation methods for GNNs is still largely underexplored.

1.2 Main Contributions

In this paper, we introduce *Prototype-based GNN-Explainer (PAGE)*, a novel *post-hoc* model-level explanation method that explains what the underlying GNN model has learned for graph classification by discovering human-interpretable *prototype graphs*. The GNN model’s behavior is represented as the prototype graphs by identifying graph patterns that the model has learned for a given target class. We formulate our problem guided by the following insight: the common graph pattern that we shall seek is indeed within the training set. Thus, as input of PAGE, we use the training set as well as representations generated by the pre-trained GNN model in order to precisely capture what the model has learned. Fig. 1 illustrates an example where PAGE correctly identifies the benzene structure from the set of molecules as the resulting model-level explanation, while using a set of both node-level and graph-level embeddings through the pre-trained GNN model as input.

We aim to devise our PAGE method according to the following design principles: an explanation module itself should (a) be interpretable and (b) not be accompanied with advanced learning models (i.e., black-box learning models). Towards this end, we design a two-phase method consisting of 1) clustering and selection of embeddings on the graph-level embedding space and 2) discovery of the prototype graph. In Phase 1, we select class-distinctive graphs from the training set by performing clustering on the graph-level embedding space and then choosing k embeddings near the centroid of each cluster. This phase is motivated by claims that 1) graph-level embeddings manifesting common subgraph patterns tend to be co-located on the graph-level embedding space (which is validated empirically) and 2) the selected k graphs (or equivalently, graph-level embeddings) near the centroid can be good representations of the belonging cluster. In Phase 2, as our explanation, we discover the prototype graph from the selected k graphs.

However, representing the GNN’s behavior as a precise subgraph pattern from the selected k graphs is challenging since it requires combinatorial search over all possible k nodes across k different graphs that should collectively embody what the model has learned. To guide this search, we newly characterize a *prototype scoring* function, which is used for efficiently calculating the matching score among k nodes across k selected graphs using node-level embedding vectors. By applying the function to all possible combinations of k nodes, we iteratively search for high matching node tuples until we discover a subgraph. It is worth noting that the impacts and benefits of leveraging the two types of embedding spaces (i.e., node-level and graph-level embedding spaces) in prototype discovery are two-fold: 1) the behavior of the pre-trained GNN model is encoded to vector representations on low-dimensional embedding spaces, which can be handled readily, and 2) the rich attribute and topological information can be fused into vector representations.

To validate the quality and effectiveness of our PAGE method, we comprehensively perform empirical evaluations using various synthetic and real-world datasets. However, evaluation of model-level explanations poses another challenge as it has yet been largely underexplored in the literature. In our study, as one of main contributions, we device systematic evaluations for model-level GNN explanations, which are summarized below. First, we perform a *qualitative* evaluation by visualizing the explanations, which demonstrates that PAGE produces prototype graphs similar to the ground truth explanations. Second, by adopting two performance metrics, consistency and faithfulness [19], with modifications, we carry out the *quantitative* analysis, which (a) shows the superiority of PAGE over XGNN [17], the state-of-the-art GNN explanation method, and (b) is in agreement with the qualitative assessment. Third, we investigate the relationship between our PAGE method and instance-level explanation methods. To this end, we present two quantities, including the concentration score and relative training gain, and quantitatively assess how much instance-level explanations agree with the prototype graph discovered by PAGE. Fourth, we analyze the robustness of PAGE by visualizing the resultant prototype graphs in a more difficult setting where each training set is composed of only a few available graphs as input of PAGE; we demonstrate that reasonable ground truth explanations can still be produced. Finally, we empirically validate the effectiveness of our prototype scoring function, which successfully approximates computationally expensive alternatives.

Additionally, we would like to address the key differences of PAGE from XGNN [17]: 1) usage of *interpretable* components without black-box learning modules and 2) *generalization* ability in the sense of applying our method to diverse domains without domain-specific prior knowledge. The main technical contributions of this paper are five-fold and summarized as follows:

- We propose PAGE, a novel model-level GNN explanation method for graph classification, which is comprised of 1) clustering and selection of graph-level embeddings and 2) prototype discovery;
- We justify the usage of clustering of graph-level em-

Notation	Description
\mathcal{G}	Set of graphs
G_i	The i -th graph in \mathcal{G}
\mathcal{V}_i	Set of nodes in G_i
\mathcal{E}_i	Set of edges in G_i
\mathcal{X}_i	Set of feature vectors of nodes in \mathcal{V}_i
\mathcal{C}	Set of classes
$\mathcal{G}_{\text{proto}}^{(c)}$	Set of prototype graphs for a target class c
f_{GNN}	Pre-trained GNN model
$\mathcal{N}_{G_i}(v)$	Set of neighbors of node v in G_i
\mathbf{h}_i^j	Node-level embedding vector of node v_i^j
\mathbf{h}_{G_i}	Graph-level embedding vector of G_i
$\mathcal{H}_{G_i}^{(c)}$	Set of node-level embedding vectors in \mathcal{V}_i
$\mathcal{H}_{\mathcal{G}}^{(c)}$	Subset of graph-level embedding vectors that f_{GNN} predicts as class c
$\mathcal{H}_{\mathcal{G};l}^{(c)}$	Subset of $\mathcal{H}_{\mathcal{G}}^{(c)}$ assigned to l -th cluster
\mathcal{K}_l	Subset of \mathcal{G} corresponding to $\mathcal{H}_{\mathcal{G};l}^{(c)}$

TABLE 1: Summary of notations.

beddings in PAGE via our theoretical and empirical validation;

- To capture the general behavior of GNN models, we design a new prototype graph discovery algorithm in PAGE alongside our own prototype scoring function;
- Through our systematic evaluations, we comprehensively validate the quality of the proposed PAGE method using five graph classification datasets;
- We validate the effectiveness of PAGE in terms of the robustness to incomplete datasets and the computational efficiency.

1.3 Organization and Notations

The remainder of this paper is organized as follows. In Section 2, we present prior studies related to our work. In Section 3, we explain the methodology of our study, including the basic settings, description of GNN models, our problem formulation, and an overview of our PAGE method. Section 4 describes technical details of the proposed method. Comprehensive experimental results are shown in Section 5. Finally, we provide a summary and concluding remarks in Section 6.

Table 1 summarizes the notation that is used in this paper. This notation will be formally defined in the following sections when we present our methodology and the technical details.

2 RELATED WORK

We first summarize broader research lines related to explanation methods for deep neural networks, and then we focus on reviewing explanation methods for GNNs.

2.1 Explanation Methods for Deep Learning

Significant research efforts have been made on interpretation techniques that explain deep neural network models on image data. While existing techniques are commonly partitioned into instance-level and model-level methods,

considerable attention has been paid to instance-level explanations that explain the prediction for a given input instance by discovering salient features in the input through the underlying explainable method. As one of the earliest instance-level explanation methods, sensitivity analysis (SA) was presented in [20] by providing a gradient heatmap for a given input instance as the explanation. Guided backpropagation (GBP) [21] was also proposed as another gradient-based explanation approach. As one of widely used techniques, layer-wise relevance propagation (LRP) [22] and its variants [23], [24] were shown by devising redistribution rules such that the model output values are redistributed proportionally to the activation values in forward propagation. Besides, Grad-CAM [25] was presented by producing explanations based on a coarse heatmap highlighting salient regions in the given image. Instead of heatmap-based explanations, LIME [4] was designed as an interpretable surrogate model such as linear regression and decision tree models.

In contrast to the instance-level explanations, model-level explanation methods [26], [27], [28] aim at offering the interpretability of the underlying model itself. These methods generally generate the optimized input in the sense of maximizing a certain prediction score (e.g., a class score) that the given explanation model produces. For example, experiments in [26], built upon generating unrealistic images that can fool convolutional neural network (CNN) models, demonstrated that there exists a difference between human and deep learning-based visual perceptions. As a more sophisticated method, DGN-AM [27] was introduced by employing another neural network architecture trained to invert feature representations of an arbitrary layer of a target model in order to produce realistic images. Motivated from the fact that the images generated from [27] do not meet sample diversity on images, PPGN [28] was developed by adding a learned prior to generate realistic high-resolution images exhibiting more diversity.

2.2 Explanation Methods for GNNs

Even with the great success of GNN models in solving various graph mining tasks such as node/graph classification [1], much less attention has been yet paid to the study on *explaining* GNN models. As an earlier attempt, the application of existing explanation methods such as SA [20], GBP [21], and LRP [22] to graph convolutional network (GCN) [29], one of the first and most popular models for GNNs, was studied in [5] for both node and graph classification tasks. However, such methods have inherent limitations due to the fact that models suitable for data with Euclidean or grid-like structures (e.g., images) cannot be straightforwardly applied to graph-structured data in a non-Euclidean space. For GNN models, explanations as a form of *subgraphs* rather than heatmaps would be appropriate. As a recent study, GNNExplainer [6] was developed to discover a subgraph, including the target node, to be explained by maximizing the mutual information between prediction values of the original graph and the discovered subgraph. GNN-LRP [11] extended the idea of LRP to GNN models to produce higher-order explanations via relevant walks contributing to the model decisions. CoGE [7] was

proposed based on contrastive explanations by finding similarities to graphs with the same label and dissimilarities to graphs with different labels. In [8], SubgraphX identified the most relevant subgraph explaining the model prediction via Monte Carlo tree search using Shapley values as a measure of subgraph importance. On the other hand, instead of directly searching for subgraphs, several studies [9], [10], [12] were shown to learn parameterized models for explanations of GNN’s predictions. PGExplainer [9] proposed a probabilistic graph generative model to provide explanations of multiple instances collectively. GraphMask [10] also proposed a post-hoc method that interprets the predictions determining whether (superfluous) edges at every GNN layer can be removed. As a causal learning approach, Gem [12] presented an explanation model equipped with a loss function based on the notion of Granger causality [30]. Furthermore, PGM-Explainer [13] presented a probabilistic graphical model so as to provide an explanation by investigating predictions of GNNs when the GNN’s input is perturbed. In RC-Explainer [15], a reinforcement learning agent was presented to construct an explanatory subgraph by adding a salient edge to connect the previously selected subgraph at each step, where a reward is obtained according to the causal effect for each edge addition. Most recently, CF-GNNExplainer [14] presented a counterfactual explanation in the form of minimal perturbation to the input graph such that the model prediction changes.

It is worth noting that, although there have been the aforementioned recent attempts to design *instance-level* explanation methods for GNN models (e.g., [5], [6], [9], [13]), *model-level* explanations for GNNs have been largely underexplored in the literature. XGNN [17] was developed only for model-level GNN explanations, where a subgraph pattern that maximizes the target class probability is generated via a reinforcement learning framework.

2.3 Discussion

Apart from most explanation methods providing explanations given a graph instance, we aim at designing model-level interpretations that rather offer not only high-level insights but also generic understandings of the underlying model mechanism. Despite the fact that XGNN [17] is known to be only one model-level explanation method in the literature, the method poses several practical challenges. First, XGNN requires domain knowledge to provide appropriate rewards in the graph generation procedure based on reinforcement learning. Second, if the reward function is not carefully designed due to the lack of domain knowledge, then the generated representative graph would be hardly realistic. This motivates us to design a more interpretable and convenient model-level method with no need of domain-specific knowledge.

3 METHODOLOGY

In this section, we first describe our problem setting with the objective. Then, we present the overview of our PAGE method as a model-level explanation for GNNs.

3.1 Settings and Basic Assumptions

Let us assume that we are given a set of n graphs $\mathcal{G} = \{G_i\}_{i=1}^n$ with node attributes. Each graph is denoted as $G_i = (\mathcal{V}_i, \mathcal{E}_i, \mathcal{X}_i)$, where $\mathcal{V}_i = \{v_i^1, \dots, v_i^{|\mathcal{V}_i|}\}$ is the set of nodes with cardinality $|\mathcal{V}_i|$ and \mathcal{E}_i is the set of edges between pairs of nodes in \mathcal{V}_i . We assume each graph G_i to be undirected and unweighted without self-edges or repeated edges. We define $\mathcal{X}_i = \{\mathbf{x}_i^1, \dots, \mathbf{x}_i^{|\mathcal{V}_i|}\}$ as the set of feature (attribute) vectors of nodes in \mathcal{V}_i , where $\mathbf{x}_i^j \in \mathbb{R}^d$ is the feature vector of node v_i^j in G_i and d is the number of features per node.

We associate each graph G_i with a label y_i , where y_i is an element in the set $\mathcal{C} = \{c_1, \dots, c_m\}$, which means that we deal with an m -class graph classification problem. Finally, a pre-trained GNN model $f_{\text{GNN}} : \mathcal{G} \rightarrow \mathcal{C}$ for graph classification corresponds to the model of interest to be explained.

3.2 GNN Models for Graph Classification

In this subsection, we give a brief review of GNN models for graph classification. We refer to [31] for more detailed description.

First, we show a general form of message passing in GNNs, in which we iteratively update the representation of a node by aggregating representations of its neighbors using two functions. Specifically, given a graph G_i , the underlying GNN model produces the latent representation vector \mathbf{u}_v^p of node $v \in \mathcal{V}_i$ at the p -th GNN layer, where $p \in \{1, \dots, P\}$.¹ Formally, the p -th layer of the GNN model updates the latent representation \mathbf{u}_v^p of each node v in \mathcal{V}_i by passing through two phases, including the message passing phase and the update phase, which are expressed as

$$\mathbf{m}_v^{p+1} = \sum_{v' \in \mathcal{N}_{G_i}(v)} M_p(\mathbf{u}_v^p, \mathbf{u}_{v'}^p), \quad (1)$$

$$\mathbf{u}_v^{p+1} = U_p(\mathbf{u}_v^p, \mathbf{m}_v^{p+1}), \quad (2)$$

respectively, where $\mathcal{N}_{G_i}(v)$ indicates the set of neighbors of node v in the given graph G_i . Here, the message function $M_p(\cdot, \cdot)$ and the update function $U_p(\cdot, \cdot)$ can be specified by several types of GNN models.² After passing through all P layers, we acquire the final representation as the *node-level* embedding vector of node v_i^j , which is denoted as $\mathbf{h}_i^j = \mathbf{u}_{v_i^j}^P \in \mathbb{R}^b$ for the dimension b of each vector.

Second, we describe how to produce the *graph-level* embedding vector \mathbf{h}_{G_i} of G_i by passing through a readout function $R(\cdot)$ that collects all node-level embedding vectors \mathbf{h}_i^j for $v_i^j \in \mathcal{V}_i$, which is formally expressed as

$$\mathbf{h}_{G_i} = R(\mathcal{H}_{G_i}), \quad (3)$$

where $\mathcal{H}_{G_i} = \{\mathbf{h}_i^j | v_i^j \in \mathcal{V}_i\}$, indicating the set of embedding vectors of nodes in \mathcal{V}_i . Here, differentiable permutation-invariant functions such as the summation and average [2]

1. To simplify notations, v_i^j will be written as v unless dropping the superscript j and the subscript i causes any confusion.

2. As an example, GCN [29] can be implemented by using $M_p(\mathbf{u}_v^p, \mathbf{u}_w^p) = (\sqrt{\deg(v)\deg(w)})^{-1/2} \mathbf{u}_w^p$ and $U_p = \sigma(W^p \cdot \mathbf{m}_v^{p+1})$, where $\deg(\cdot)$ is the degree of each node and $\sigma(\cdot)$ is the activation function.

are typically used as the readout function. Then, the set of calculated graph-level embedding vectors over all graphs \mathcal{G} is fed into a classifier to perform graph classification.

3.3 Problem Formulation

The objective of our study is to provide a post-hoc *model-level* explanation by discovering the most distinctive graph patterns that the underlying GNN model has learned during training for graph classification. Towards this end, we present PAGE, a new model-level explanation method along with human-interpretable *prototype* graphs. For a target class $c \in \mathcal{C}$ to which a given graph belongs and a pre-trained GNN model f_{GNN} , PAGE aims to discover a set of prototype graphs, $\mathcal{G}_{\text{proto}}^{(c)}$, each of which represents the graph pattern such that the model f_{GNN} most likely predicts the target class c . Formally, the model-level explanation function $f_{\text{model}}^X(\cdot, \cdot)$ in PAGE is expressed as:

$$\mathcal{G}_{\text{proto}}^{(c)} = f_{\text{model}}^X(c; f_{\text{GNN}}). \quad (4)$$

Note that the model-level explanation differs from the instance-level explanation, which provides an explanation with respect to a given graph instance $G_i \in \mathcal{G}$ rather than a target class.

3.4 Overview of Our PAGE Method

In this subsection, we explain our methodology along with the overview of the proposed PAGE method, which is basically composed of the following two phases: 1) selection of input graphs that precisely represent the given class c through clustering and selection of graph-level embeddings, and 2) discovery of the prototype graph set $\mathcal{G}_{\text{proto}}^{(c)}$.

Before describing each phase above, let us state the core difference from XGNN [17], the state-of-the-art model-level explanation method for GNNs. While XGNN was designed to *generate* the prototype graph, PAGE attempts to *discover* the set of prototype graphs, $\mathcal{G}_{\text{proto}}^{(c)}$, using underlying graphs, \mathcal{G} , by turning our attention to both the graph-level and node-level embedding spaces. Training a generative model in [17] for obtaining the prototype graph has several downsides since it not only requires a judicious design of the reward function based on domain knowledge but is also sensitive to the initial graph fed to the generator. In contrast, when we discover $\mathcal{G}_{\text{proto}}^{(c)}$ within the set of graphs, the impacts and benefits of leveraging the two types of embedding spaces are two-fold. First, the behavior of the pre-trained GNN model is encoded to vector representations on low-dimensional embedding spaces, thus facilitating many network analysis tasks. Second, the rich attribute and structural information of \mathcal{G} can be efficiently and effectively fused into vector representations in conducting the prototype discovery. In particular, the set of graph-level embedding vectors can be used to reduce the prototype graph search space within the set \mathcal{G} by selecting only a small number of embedding vectors that are most representative.

Now, we describe each phase of our PAGE method as follows. First, we select a small number of graphs from the input that represent the given class c by performing clustering on the graph-level embedding space (see the left

part in Fig. 2a). This phase is motivated by the observation that graph-level embedding vectors revealing common subgraph patterns tend to be co-located on the graph-level embedding space (which will be empirically shown in Section 4.1.2). The clustering phase also provides a practical advantage, where it provides a natural anchor point to which we select graph-level embedding vectors (and their corresponding graphs) as the centroid of each cluster. For a target class c , we focus on $\mathcal{H}_{\mathcal{G}}^{(c)}$, which is defined as a subset of graph-level embedding vectors such that the model f_{GNN} predicts as class c . In this phase, we discover L clusters using a Gaussian mixture model (GMM) [32] for a pre-defined parameter L . To this end, we estimate the parameters $\{(\pi_l, \mu_l, \Sigma_l)\}_{l=1}^L$, indicating the mixing coefficient π_l , the mean vector μ_l , and the covariance matrix Σ_l of the Gaussian mixture distribution to fit the embedding vectors $\mathcal{H}_{\mathcal{G}}^{(c)}$. As a result of clustering, we are capable of mapping each graph-level embedding vector to one of L clusters by dividing the set $\mathcal{H}_{\mathcal{G}}^{(c)}$ into L disjoint subsets $\mathcal{H}_{\mathcal{G};1}^{(c)}, \dots, \mathcal{H}_{\mathcal{G};L}^{(c)}$, where $\mathcal{H}_{\mathcal{G};l}^{(c)}$ denotes the set of graph-level embedding vectors in $\mathcal{H}_{\mathcal{G}}^{(c)}$ assigned to the l -th cluster. After acquiring L clusters, we select the k -nearest neighbors (k NNs) from each cluster's centroid on the graph-level embedding space for a pre-defined parameter k . Since centroids are typically around the center of each cluster, graph-level embedding vectors near centroids can be thought of as good representations of the belonging clusters. More specifically, by measuring the Mahalanobis distance between the graph-level embedding vector $\mathbf{h}_{G_i} \in \mathcal{H}_{\mathcal{G};l}^{(c)}$ and the mean vector μ_l within the l -th cluster, we select the k NNs among the vectors in $\mathcal{H}_{\mathcal{G};l}^{(c)}$ from μ_l . Afterwards, we acquire \mathcal{K}_l , which represents the subset of underlying graphs in \mathcal{G} corresponding to k selected graph-level embedding vectors. That is, we retrieve a subset of graphs from the selected graph-level embedding vectors. Fig. 2b illustrates an example of retrieving $\mathcal{K}_1 = \{G_1, G_2, G_3\}$ using the 3-nearest neighbors \mathbf{h}_{G_1} , \mathbf{h}_{G_2} , and \mathbf{h}_{G_3} from the centroid when $k = 3$.

Second, we turn to discovering the prototype graph (see the right part in Fig. 2a). For the ease of explanation, we focus only on the l -th cluster. Given $\mathcal{K}_l = \{G_1, \dots, G_k\}$ for the l -th cluster, we aim to discover a common subgraph pattern within the subset \mathcal{K}_l , which serves as the prototype graph, denoted as $g_l^{(c)}$, in the set $\mathcal{G}_{\text{proto}}^{(c)}$. To this end, we create an order- k tensor (i.e., a k -dimensional array) $\mathbf{Y}_l \in \mathbb{R}^{|\mathcal{V}_1| \times \dots \times |\mathcal{V}_k|}$ to compare nodes across k different graphs in \mathcal{K}_l in order to select the most probable nodes that embrace the common subgraph pattern, where each element of \mathbf{Y}_l represents the *matching score* among k nodes, which will be formalized in the next section. By taking advantage of the structural and attribute information embedded by the model f_{GNN} , we calculate the matching score among k nodes, i.e., the element $\mathbf{Y}_l[i_1, \dots, i_k]$, which measures how high the matching score for the node-level embedding vectors of nodes $v_1^{i_1}, \dots, v_k^{i_k}$ is. From the tensor \mathbf{Y}_l , we iteratively search for k -tuples of nodes until we are ready for discovering a subgraph, where each element of the selected k -tuple corresponds to a single node in the common subgraph that we want to discover (refer to Section 4.2.3 for more details). Afterwards, we extract a subgraph by only

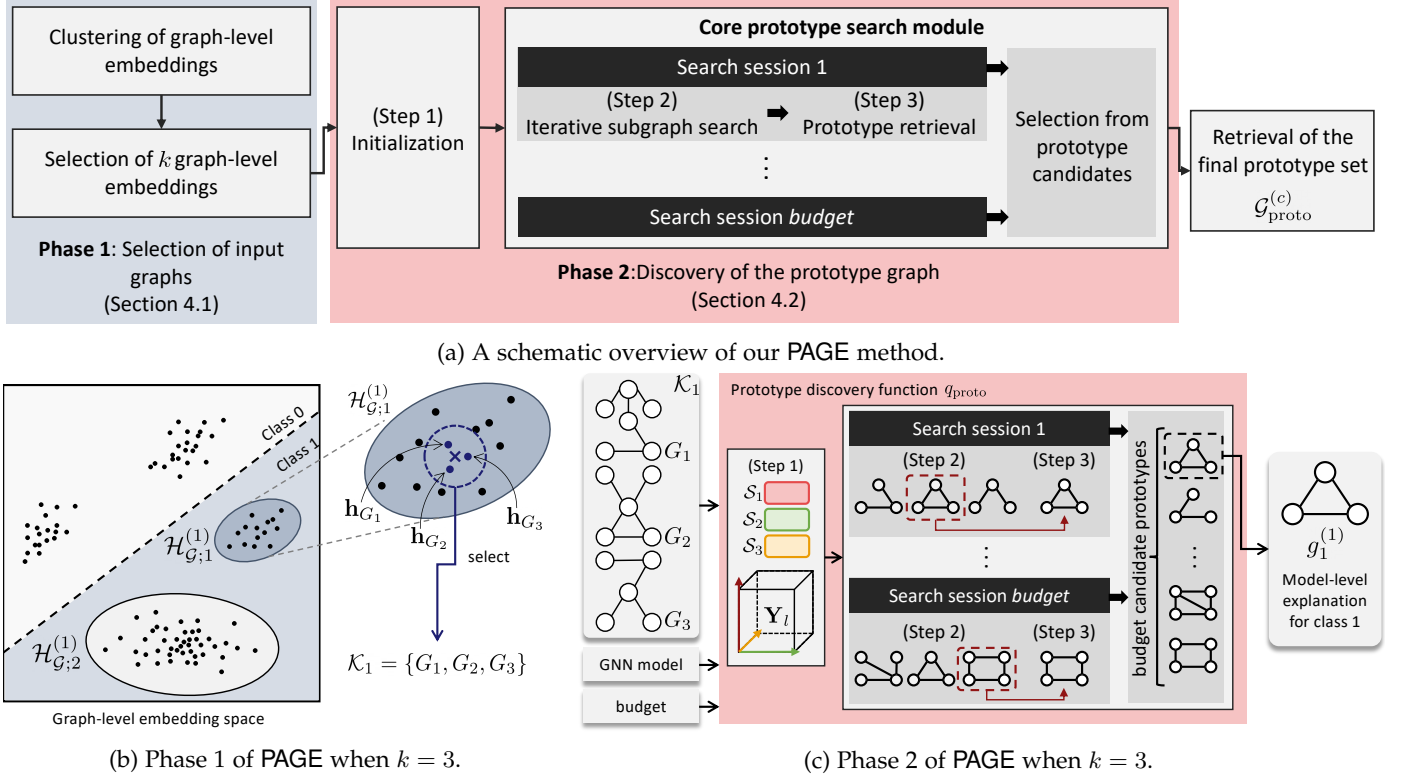


Fig. 2: A schematic overview overview and an illustrative example of our PAGE method.

taking into account the set of nodes found over iterations. Then, we are capable of calculating the output probability p_{GNN} for each subgraph extracted from k graphs in the set \mathcal{K}_l by feeding each into f_{GNN} , where the subgraph with the highest p_{GNN} is selected. The procedure of subgraph search starts by finding k -tuples of nodes corresponding to the highest matching score in \mathbf{Y}_l . Nevertheless, so as to enhance the possibility of retrieving a reliable prototype graph, we continue on with finding another set of k nodes such that the second highest matching score in \mathbf{Y}_l is returned; we repeat this procedure during multiple search sessions alongside a given *search budget*. Finally, the subgraph exhibiting the highest p_{GNN} among the ones found across all search sessions is retrieved as the resulting prototype graph, which provides an intuitive model-level explanation for GNN’s prediction given the target class c . Fig. 2c illustrates an example of retrieving the final prototype graph $g_1^{(1)}$ based on the prototype discovery function q_{proto} using $\mathcal{K}_1 = \{G_1, G_2, G_3\}$ as input.

4 PAGE: PROPOSED METHOD

In this section, we elaborate on PAGE, the proposed post-hoc model-level GNN explanation method for graph classification. We first describe how to cluster and select graph-level embeddings for the subset selection of input graphs in detail. We also provide the theoretical and empirical validation for our clustering. Then, we present how to discover prototype graphs. The overall procedure of our PAGE method is summarized in Algorithm 1 in which the prototype search function $q_{\text{proto}}(\cdot, \cdot, \cdot)$ is invoked to return the prototype graph set $\mathcal{G}_{\text{proto}}^{(c)} = \{g_l^{(c)}\}_{l=1}^L$.

Algorithm 1 : PAGE

Input: $f_{\text{GNN}}, \mathcal{G}, L, c, \text{budget}$

Output: $g_1^{(c)}, \dots, g_L^{(c)}$

- 1: Acquire $\mathcal{H}_{\mathcal{G}}^{(c)}$ using f_{GNN} and \mathcal{G}
- 2: $\{(\pi_l, \mu_l, \Sigma_l)\}_{l=1}^L \leftarrow \text{GMM}(\mathcal{H}_{\mathcal{G}}^{(c)}, L)$
- 3: **for** $l = 1, \dots, L$ **do**
- 4: $\mathcal{K}_l \leftarrow k\text{NN}(k, \mathcal{H}_{\mathcal{G}}^{(c)}, \mathcal{G}, \mu_l, \Sigma_l)$
- 5: $g_l^{(c)} \leftarrow q_{\text{proto}}(\mathcal{K}_l, f_{\text{GNN}}, \text{budget})$
- 6: **end for**
- 7: $\mathcal{G}_{\text{proto}}^{(c)} \leftarrow \{g_1^{(c)}, \dots, g_L^{(c)}\}$
- 8: **return** $\mathcal{G}_{\text{proto}}^{(c)}$

4.1 Clustering and Selection of Graph-Level Embeddings (Phase 1)

4.1.1 Methodological Details

We assume that parameters of a GNN model f_{GNN} are trained by a set of graphs, \mathcal{G} . Given a target class $c \in \mathcal{C}$, we obtain a set of graph-level embedding vectors, $\mathcal{H}_{\mathcal{G}}^{(c)}$, through a feed-forward process of GNN (see line 1 in Algorithm 1).

Then, we estimate the parameters of the Gaussian mixture distribution to fit the embedding vectors $\mathcal{H}_{\mathcal{G}}^{(c)}$. More precisely, we apply an expectation maximization (EM) algorithm [33] to estimate the parameters $\{(\pi_l, \mu_l, \Sigma_l)\}_{l=1}^L$ with the mean vector μ_l and the covariance matrix Σ_l for the l -th cluster of the Gaussian mixture distribution $p(\mathbf{h}) = \sum_{l=1}^L \pi_l \mathcal{N}(\mathbf{h} | \mu_l, \Sigma_l)$ (see line 2 in Algorithm 1). The EM iteration alternates between performing the E-step and M-step as follows. In the E-step, we calculate $\gamma_{nl}^{(t)}$, which

represents the posterior probability of the n -th vector in $\mathcal{H}_G^{(c)}$ being assigned to the l -th cluster and is expressed as

$$\gamma_{nl}^{(t)} = \frac{\pi_l \mathcal{N}(\mathbf{h}_{G_n} | \boldsymbol{\mu}_l^{(t)}, \boldsymbol{\Sigma}_l^{(t)})}{\sum_{i=1}^L \pi_i \mathcal{N}(\mathbf{h}_{G_n} | \boldsymbol{\mu}_i^{(t)}, \boldsymbol{\Sigma}_i^{(t)})}, \quad (5)$$

where the superscript (t) indicates the EM iteration index. In the M-step, we re-estimate the GMM parameters:

$$\begin{aligned} \boldsymbol{\mu}_l^{(t+1)} &= \frac{1}{N_l} \sum_{n=1}^{|\mathcal{H}_G^{(c)}|} \gamma_{nl}^{(t)} \mathbf{h}_{G_n}, \\ \boldsymbol{\Sigma}_l^{(t+1)} &= \frac{1}{N_l} \sum_{n=1}^{|\mathcal{H}_G^{(c)}|} \gamma_{nl}^{(t)} (\mathbf{h}_{G_n} - \boldsymbol{\mu}_l^{(t+1)}) (\mathbf{h}_{G_n} - \boldsymbol{\mu}_l^{(t+1)})^T, \end{aligned} \quad (6)$$

$$(7)$$

where $N_l = \sum_{n=1}^{|\mathcal{H}_G^{(c)}|} \gamma_{nl}^{(t)}$. Using the estimated parameters, we assign each graph-level embedding vector \mathbf{h}_{G_i} to the cluster with the highest probability $\gamma_{nl}^{(t)}$. In other words, we divide $\mathcal{H}_G^{(c)}$ into L disjoint subsets $\mathcal{H}_{G;1}^{(c)}, \dots, \mathcal{H}_{G;L}^{(c)}$, where $\mathcal{H}_{G;i}^{(c)}$ contains graph-level embedding vectors assigned to the i -th cluster by the GMM.

Next, we select the k NNs from each cluster's centroid on the graph-level embedding space in order to find the set of k graphs, \mathcal{K}_l , for each cluster (see line 4 in Algorithm 1). To this end, we sort the vectors \mathbf{h}_{G_i} in descending order with respect to the Mahalanobis distance from the mean vector $\boldsymbol{\mu}_l$ within the l -th cluster [32]:

$$((\mathbf{h}_{G_i} - \boldsymbol{\mu}_l)^T \boldsymbol{\Sigma}_l^{-1} (\mathbf{h}_{G_i} - \boldsymbol{\mu}_l))^{1/2}. \quad (8)$$

Then, for each cluster, we select k graph-level embedding vectors that are closest to $\boldsymbol{\mu}_l$ and their corresponding input graphs \mathcal{K}_l in \mathcal{G} .

4.1.2 Theoretical and Empirical Validation

In Section 4.1.2, we aim at justifying the usage of clustering of graph-level embeddings in PAGE via our theoretical and empirical validation. Our study basically presumes that graphs containing different prototypes are highly likely to be mapped into different vector representations on the graph-level embedding space, even though they belong to the same class. To validate this claim, we first provide a theoretical foundation that connects GNNs and the *Weisfeiler-Lehman (WL) kernel* [34] in the sense of performing the *graph classification* task, where the WL kernel is capable of differentiating graphs according to their structures regardless of graph labels. We then empirically validate the above claim by visualizing graph-level embeddings for a benchmark dataset.

We start by describing the WL kernel, which is mostly used for *graph isomorphism* testing. Color refinement [35] is a simple yet effective algorithmic routine that determines whether two graphs are non-isomorphic. It initially colors each node of a given graph by the node attribute [36] and iteratively refines the node coloring in rounds by taking into account the colors in the neighbors of each node until stabilization. We formally state this by assuming that a graph G_i is given along with the initial color for each node. A node coloring $c^{(p)}$ is a function that bijectively maps each node $v \in \mathcal{V}_i$ in G_i to a unique color that has not

been used in previous iterations, where $p \geq 0$ indicates the iteration index. For the target node v , the WL kernel iteratively updates $c^{(p)}(v)$ by recoloring over the multiset of neighborhood colors, i.e., $\{\{c^{(p-1)}(v') | v' \in \mathcal{N}_{G_i}(v)\}\}$, where $\mathcal{N}_{G_i}(v)$ indicates the set of neighbors of node v in G_i .³ Now, we are ready to establish the following theorem, which verifies that there exists a GNN model equivalent to the WL kernel as long as node-level embeddings are concerned.

Theorem 1 (Morris et al., 2019). *Let $f_{\text{GNN}}^{(p)}$ denote the function that returns node-level vector representations at the p -th GNN layer in f_{GNN} . Then for all $p \geq 0$, there exists a GNN model equivalent to a node coloring such that $f_{\text{GNN}}^{(p)}(u) = f_{\text{GNN}}^{(p)}(v)$ if and only if $c^{(p)}(u) = c^{(p)}(v)$ for every $u, v \in \mathcal{V}_i$.*

From Theorem 1, the final node-level embedding vector \mathbf{h}_i^j of node v_i^j is equivalent to $c^{(P)}(v_i^j)$. Next, we turn to exploring the relationship between a GNN model and the WL kernel in discovering *graph-level* embeddings. To this end, we first acquire a graph feature vector of G_i , denoted as $\mathbf{l}_{G_i} = [n_i^1, \dots, n_i^s]$, where s is the number of unique node colors and n_i^l is the number of nodes for which color l has been assigned for $l = 1, \dots, s$. The graph feature vector \mathbf{l}_{G_i} is used to compute similarities between pairs of graphs. The following corollary states the equivalence between the GNN model and the WL kernel in terms of graph-level embeddings.

Corollary 2. *Suppose that two graph feature vectors \mathbf{l}_{G_a} and \mathbf{l}_{G_b} are obtained via color refinement for two graphs G_a and G_b , respectively. Then, for a GNN model with P layers such that $c^{(P)}$ and $f_{\text{GNN}}^{(P)}$ are equivalent, $\mathbf{l}_{G_a} = \mathbf{l}_{G_b}$ implies $R(\mathcal{H}_{G_a}) = R(\mathcal{H}_{G_b})$, when $R(\cdot)$ is either the summation or average function.*

Proof. From Theorem 1, there exists a bijective function $\nu : c^{(P)}(v_i^j) \rightarrow \mathbf{h}_i^j$ for node $v_i^j \in \mathcal{V}_i$, where i is either a or b . Moreover, $\mathbf{l}_{G_a} = \mathbf{l}_{G_b}$ indicates that both the number of nodes and the distribution of node colors over each graph are the same for G_a and G_b . Due to the fact that each node-level embedding vector \mathbf{h}_i^j can be regarded as a bijection ν of a node color, the distributions of unique node-level embedding vectors for G_a and G_b are identical. In this context, if the readout function $R(\cdot)$ is the summation, then we have

$$\sum_{j=1}^{|\mathcal{V}_a|} \mathbf{h}_a^j = \sum_{j'=1}^{|\mathcal{V}_b|} \mathbf{h}_b^{j'}, \quad (9)$$

thus resulting in $R(\mathcal{H}_{G_a}) = R(\mathcal{H}_{G_b})$, since the summation is permutation-invariant. When $R(\cdot)$ is given by the average function, this corollary can also be proven by dividing each side of (9) by the number of nodes. This completes the proof of this corollary. \square

From Corollary 2, one can expect that GNNs will behave as WL kernels in the sense of differentiating graphs (i.e., distinguishing non-isomorphic graphs).

Next, we empirically validate our claim that GNNs can differentiate graphs containing different prototypes.

3. A multiset is a generalized version of a set that allows multiple instances for each of its elements, where the multiplicity of each element in the multiset corresponds to the number of instances.

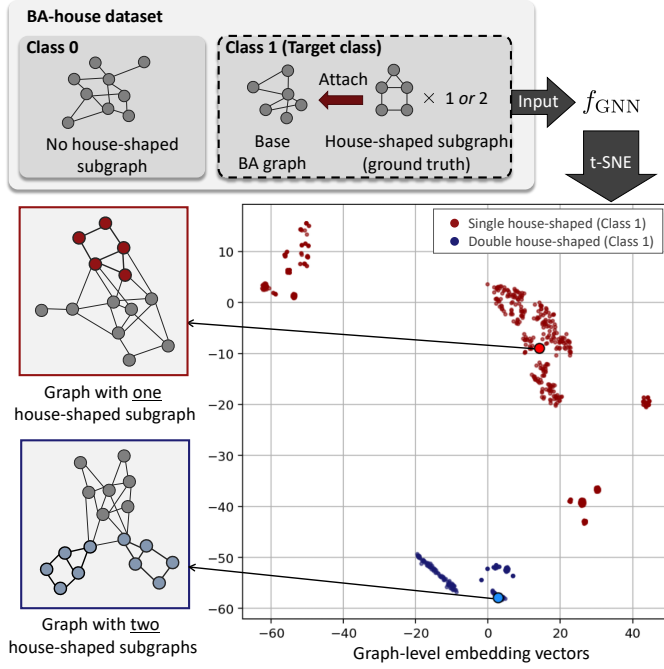


Fig. 3: Visualization of graph-level embeddings for the BA-house dataset.

Example 1. In Fig. 3, to show such a tendency in practice to some degree, we visualize graph-level embedding vectors for the BA-house dataset in which there are multiple graphs with and without the house-shaped subgraph(s), where t -SNE [37] is used for visualization on the two-dimensional graph-level embedding space (refer to Section 5.1 for more description of BA-house). Here, we train a GNN model to perform a graph classification task that classifies whether an input graph contains the house-shaped subgraph(s) (Class 1) or not (Class 0). However, from the fact that each graph in Class 1 may have either one or two house-shaped subgraphs corresponding to two separate ground truth prototypes, we are interested in further investigating whether graphs with different numbers of house-shaped subgraphs, belonging to Class 1, are separately embedded into the graph-level embedding space. Although the GNN model is trained while being unaware of the existence of such prototypes, we apparently observe that the GNN model embeds input graphs with different prototypes to distant clusters in the graph-level embedding space (see red and blue points in Fig. 3).

Through this empirical validation, we conclude that GNNs are indeed capable of differentiating graphs with different prototypes as in the WL kernel.

4.2 Prototype Discovery (Phase 2)

In this section, we turn our attention to describing our prototype discovery algorithm q_{proto} (see line 5 in Algorithm 1), which calculates the matching score by comparing k nodes across k different graphs in the set $\mathcal{K}_l = \{G_1, \dots, G_k\}$. Since we iteratively discover a prototype graph $g_l^{(c)}$ for each cluster $l \in \{1, \dots, L\}$, we concentrate only on obtaining $g_l^{(c)}$ for the l -th cluster in this subsection. The prototype

discovery phase consists of the initialization step and the core prototype search module that is made up of two steps. The mechanism of the core prototype search module for a certain search session is illustrated in Fig. 4 where the parameter k in k NN is given by 3.

4.2.1 Initialization (Step 1)

The initialization step is composed of the creation of an order- k matching tensor \mathbf{Y}_l and the creation of empty node lists. We first describe how to create \mathbf{Y}_l . From the set of node-level embedding vectors, $\mathcal{H}_{G_i} \in \mathbb{R}^{|\mathcal{V}_i| \times b}$ for each $G_i \in \mathcal{K}_l$, we are interested in calculating the order- k tensor \mathbf{Y}_l , where each element of \mathbf{Y}_l is the matching score among k nodes (see the block of Iteration 0 in Fig. 4 for $k = 3$). To take into account node-level embedding vectors from f_{GNN} in efficiently calculating the matching score, we formally define a new scoring function:

Definition 1 (Prototype scoring function). Given a set of b -dimensional vectors $\{\mathbf{v}_i\}_{i=1}^k$, we define the *prototype scoring function* $s : \mathbb{R}^b \times \dots \times \mathbb{R}^b \rightarrow \mathbb{R}$ as follows:

$$s(\mathbf{v}_1, \dots, \mathbf{v}_k) = \mathbf{1}^T (\mathbf{v}_1 \odot \dots \odot \mathbf{v}_k), \quad (10)$$

where \odot indicates the element-wise product and $\mathbf{1} \in \mathbb{R}^b$ is the all-ones vector.

We now focus on calculating each element of \mathbf{Y}_l by using the node-level embeddings as input of the prototype scoring function s . To this end, we first denote $\mathbf{X}_l \in \mathbb{R}^{|\mathcal{V}_1| \times \dots \times |\mathcal{V}_k|}$ as another order- k tensor such that $\mathbf{X}_l[i_1, \dots, i_k] \triangleq s(\mathbf{h}_{G_1}^{i_1}, \dots, \mathbf{h}_{G_k}^{i_k})$. Each element of \mathbf{X}_l represents a matching score that encodes the likelihood that k nodes, each of which comes from the corresponding k graphs in the set \mathcal{K}_l , match well on the node-level embedding space according to the GNN model f_{GNN} . In order to normalize \mathbf{X}_l and encode additional information, we then obtain \mathbf{Y}_l by going through two operations $u_{k'}^1(\cdot)$ and $u_{k'}^2(\cdot)$ on \mathbf{X}_l for $k' \in \{1, \dots, k\}$ that modify the values of the input tensor while not changing the dimensions: 1) $u_{k'}^1(\mathbf{X}_l)$ applies the softmax normalization along the k' -th dimension; and 2) $u_{k'}^2(\mathbf{X}_l)$ returns the average matching score along the k' -th dimension and is expressed as $\sigma(\sum_{i_{k'}=1}^{|\mathcal{V}_{k'}|} \mathbf{X}_l[\dots, i_{k'}, \dots]) / |\mathcal{V}_{k'}|$, where $\sigma(\cdot)$ is the sigmoid function. Finally, we are capable of calculating \mathbf{Y}_l by taking the average of the element-wise products of $u_{k'}^1(\mathbf{X}_l)$ and $u_{k'}^2(\mathbf{X}_l)$ over all dimensions:

$$\mathbf{Y}_l = \frac{1}{k} \left(\sum_{k'=1}^k u_{k'}^1(\mathbf{X}_l) \odot u_{k'}^2(\mathbf{X}_l) \right). \quad (11)$$

For our matching score calculation, we would like to bring up the computational complexity issues as below.

Remark 1. Although the inner product is a natural way of encoding similarities between two node-level embedding vectors, its extension to the case of more than two vectors is not straightforward. A naïve approach would be the calculation of all possible inner products between pairs of k embedding vectors, which is however inefficient as such pairwise comparisons take $\mathcal{O}(k^2)$. On the other hand, it is possible to calculate the matching score among k nodes with a linear scaling of k (i.e., $\mathcal{O}(k)$) by using the prototype

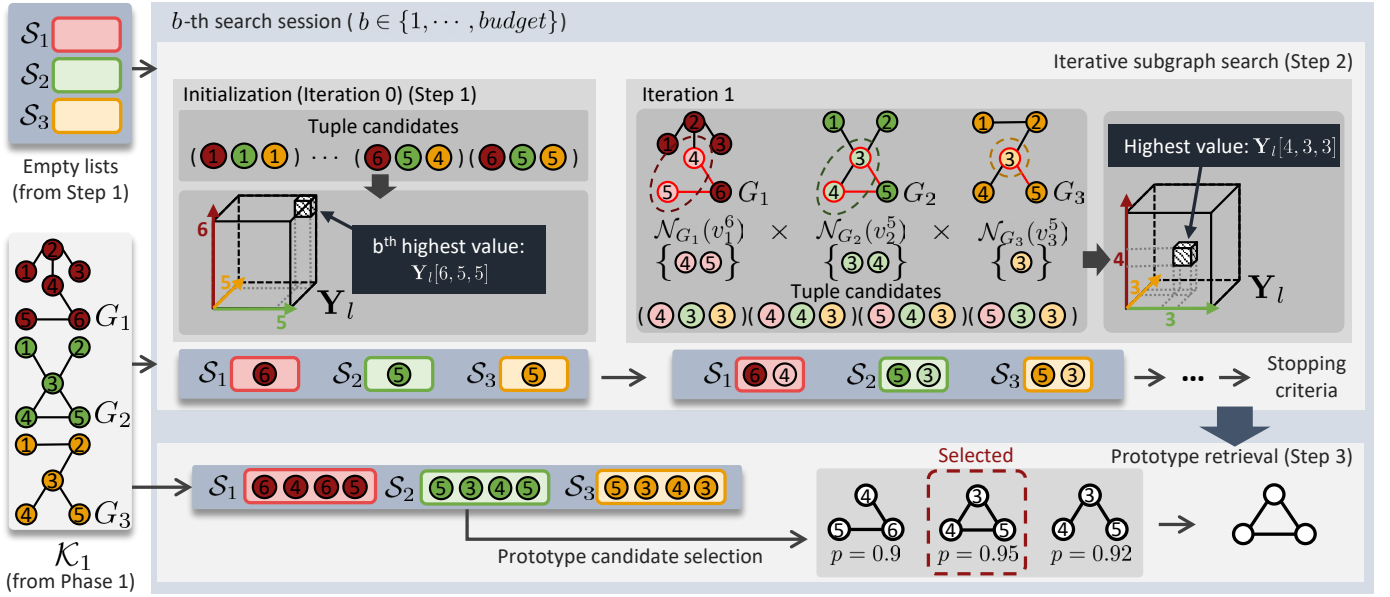


Fig. 4: An example that illustrates the mechanism of the core prototype search module for a certain search session when $k = 3$.

scoring function s in (10). Note that our prototype scoring function becomes the inner product when $k = 2$.

Remark 2. In order to reduce the search space, we are capable of excluding node tuples in the matching tensor Y_l such that the feature vectors of the corresponding nodes do not coincide. To achieve this, we post-process Y_l by assigning zeros to the elements of Y_l in which feature vectors of nodes are not identical to each other. For example, suppose that $k = 3$ along with the order-3 matching tensor Y_l in Fig. 4. For each element $Y_l[i, j, m]$, we examine the feature vectors of nodes, i.e., \mathbf{x}_1^i , \mathbf{x}_2^j , and \mathbf{x}_3^m . We do not modify the value of $Y_l[i, j, m]$ if $\mathbf{x}_1^i = \mathbf{x}_2^j = \mathbf{x}_3^m$; we assign zeros to $Y_l[i, j, m]$ otherwise. Thus, it is possible to avoid searching for such zero-injected node tuples in Y_l . This post-processing does not deteriorate the performance of PAGE while substantially reducing the computational complexity of prototype search.

Next, we create k empty node lists S_1, \dots, S_k in which node indices will be included during the iterative search. As illustrated in the top-left of Fig. 4, for $k = 3$, three empty lists S_1 , S_2 , and S_3 are being initialized. The node indices in each list after the final iteration correspond to the nodes in the prototype graph $g_l^{(c)}$.

4.2.2 Core Prototype Search Module

For the remaining part of our prototype discovery phase, we would like to materialize the prototype discovery function q_{proto} , which is designed to extract common subgraph patterns in a reliable manner. In a nutshell, as depicted in Fig. 2a, we run multiple search sessions, each producing one prototype graph candidate. After running all search sessions, we feed each prototype candidate to the underlying model f_{GNN} , and acquire the one with the highest output probability p_{GNN} as the final prototype graph. This ensures that we leverage various subgraphs as candidates for the final prototype graph, thereby increasing the chances of

retrieving a trustworthy prototype graph that conforms to the underlying GNN model.

More concretely, we introduce a search budget, denoted as the variable *budget*, which determines the number of search sessions that we run. Each search session is composed of iterative subgraph search (Step 2) and prototype retrieval (Step 3). In other words, for a given *budget*, we run up to *budget* sessions for prototype search. When the prototype search is over for all sessions, we select the one having the highest output probability p_{GNN} among the *budget* discovered subgraphs as the final prototype graph $g_l^{(c)}$ for the target class c .

4.2.3 Iterative Subgraph Search (Step 2)

We now describe the iterative subgraph search step in each search session. In this step, we iteratively find k -tuples of node indices to be inserted into the created k node lists. Each iteration starts by collecting all possible k -tuples to be selected. In Iteration 0 (i.e., initial search), all combinations of k nodes across k different graphs in the set \mathcal{K}_l are valid candidates for selection. For the rest of the iterative search process, we construct node sequences by traversing for each graph; that is, combinations only from neighbors for each of the k selected nodes in the previous iteration are valid candidates for selection (See the block of Iteration 1 in Fig. 4 for $k = 3$). Selection among the valid candidates for the k -tuples is determined based on the corresponding value in Y_l . Each k -tuple with the highest matching score is chosen out of possible combinations from the sets of neighbors of already selected nodes during the iteration process, except the initial search. For the initial search, the k -tuple with the b -th highest matching score is selected, where $b \in \{1, \dots, \text{budget}\}$ indicates the index of the search session described in Section 4.2.2. We describe this step more concretely when $k = 3$ as follows.

Example 2. For $k = 3$, as illustrated in Fig. 4, all possible tuples $(1, 1, 1), \dots, (6, 5, 5)$ are being considered as candidates for the initial search. In our example, suppose that a 3-tuple $(6, 5, 5)$ has been selected since $\mathbf{Y}_l[6, 5, 5]$ is the b -th highest matching score. In Iteration 1, we focus only on the set of neighbors for each node, which are $\mathcal{N}_{G_1}(v_1^6) = \{4, 5\}$, $\mathcal{N}_{G_2}(v_2^5) = \{3, 4\}$, and $\mathcal{N}_{G_3}(v_3^5) = \{3\}$, where $\mathcal{N}_{G_i}(v)$ is the set of neighbors of node v in G_i . Then, all possible candidates are the Cartesian product of the three sets of neighbors: $\mathcal{N}_{G_1}(v_1^6) \times \mathcal{N}_{G_2}(v_2^5) \times \mathcal{N}_{G_3}(v_3^5) = \{4, 5\} \times \{3, 4\} \times \{3\}$. In consequence, the possible node candidates are given by $(4, 3, 3)$, $(4, 4, 3)$, $(5, 3, 3)$, and $(5, 4, 3)$ as depicted in Iteration 1.

Each node index of the selected k -tuple is added to each node list $\mathcal{S}_1, \dots, \mathcal{S}_k$. After selection, we update \mathbf{Y}_l by multiplying a certain decay factor along each dimension from the selected k -tuple.⁴ The whole subgraph search iteration terminates when either the allowed maximum number of iterations is reached or the size of the resultant subgraph exceeds a pre-defined value.

4.2.4 Prototype Retrieval (Step 3)

As the next step, we are capable of discovering k subgraphs, each of which is retrieved from the node list \mathcal{S}_i for G_i . In Step 3 of prototype discovery for each search session, we describe how to retrieve a candidate of the final prototype graph by evaluating the output probabilities p_{GNN} for each discovered subgraph from the list \mathcal{S}_i . Specifically, we feed each subgraph as input to the model f_{GNN} to get p_{GNN} and choose the subgraph with the highest p_{GNN} among k subgraphs (see the bottom-right in Fig. 4 for $k = 3$).

Note that, since we run *budget* search sessions, we acquire *budget* prototype candidates. We retrieve the final prototype graph $g_l^{(c)}$ by selecting the prototype candidate having the highest output probability p_{GNN} among *budget* candidates.

5 EXPERIMENTAL EVALUATION

In this section, we first describe synthetic and real-world datasets used in the evaluation. We also present the benchmark GNN explanation method for comparison. After describing our experimental settings, we comprehensively evaluate the performance of PAGE and benchmark methods. The source code for PAGE is made publicly available online.⁵

5.1 Datasets

In our study, two synthetic datasets, including the BA-house and BA-grid datasets, and three real-world chemical datasets, including the Solubility, MUTAG, and Benzene datasets, are used for the evaluation of our proposed PAGE method. The ground truth explanations (i.e., ground truth prototypes) as well as the ground truth labels for graph classification are available for each of the five datasets. The main statistics of each dataset, including the number of

Dataset	n	$\sum_i \mathcal{V}_i$ (Avg.)	$\sum_i \mathcal{E}_i$ (Avg.)	TP
BA-house	2,000	21,029 (10.51)	62,870 (31.44)	1.000
BA-grid	2,000	29,115 (14.56)	91,224 (45.61)	0.9583
Benzene	12,000	246,993 (20.58)	523,842 (43.65)	0.9444
MUTAG	4,337	131,488 (30.32)	266,894 (61.54)	0.7247
Solubility	708	9,445 (13.34)	9,735 (13.75)	0.8717

TABLE 2: Statistics of the five datasets and test performance of the GNN model trained for each dataset, where n , $\sum_i \mathcal{V}_i$, $\sum_i \mathcal{E}_i$, and TP denote the number of graphs, the total number of nodes, the total number of edges, and the test performance of the GNN model, respectively. We also report the average number of nodes and edges per graph for each dataset in the parenthesis.

graphs, the total number of nodes, and the total number of edges, are summarized in Table 2. We describe important characteristics of the datasets.

BA-house and **BA-grid**. Inspired by [6], we generate new synthetic datasets designed for the graph classification task. In both datasets, we use the Barabási-Albert (BA) model as a backbone graph, and complete each graph by attaching certain subgraph patterns (or motifs), which serve as the ground truth explanations. Both datasets contain two classes, where one class includes the ground truth explanation(s) in the underlying graph, while another class has an incomplete subgraph pattern. We describe how to generate a single graph as follows. First, we assign the class label 0 or 1 to a graph to be generated. We then generate a backbone graph using the BA model consisting of 5 to 10 nodes. If the assigned class label is 0, then we connect additional subgraph patterns to the backbone graph. Otherwise, we connect an incomplete subgraph pattern to the backbone graph. For BA-house, the subgraph pattern is a house-shaped subgraph, while, for BA-grid, a grid-like subgraph is used. In the case of BA-house, either single or double house-shaped subgraphs are randomly added within Class 0. Each node has a one-hot encoded feature vector indicating whether the node belongs to the backbone graph, the head of the motif (i.e., the ground truth explanation), or the body of the motif, depending on the node’s position in the given graph.

Benzene [19], [38]. The Benzene dataset contains molecules, where nodes and edges represent atoms and chemical bonds, respectively. The graphs are partitioned (labeled) into two different classes with respect to the existence of the benzene structure within the molecule (i.e., the structure having a six-carbon ring as the dataset neglects the Hydrogen atom) [19]. Each node has the corresponding one-hot encoded feature vector representing one possible atom type, which can be one of Carbon, Nitrogen, Oxygen, Fluorine, Iodine, Chlorine, and Bromine.

MUTAG [39]. The MUTAG dataset contains graphs representing molecules, where nodes represent different atoms, similarly as in the Benzene dataset. The graphs are partitioned into two different classes according to their mutagenic effect on a bacterium [6], [39]. The node features are one-hot encoded vectors that represent types of atoms, including Carbon, Nitrogen, Oxygen, Fluorine, Iodine, Chlorine, Bromine, and Hydrogen. In our experiments, the

4. We have empirically found that such an update of \mathbf{Y}_l with a decay factor enables us to avoid searching for the previously selected k -tuples, resulting in a more stable subgraph search process.

5. github.com/jordan7186/PAGE.

edge labels are ignored for simplicity.

Solubility [5]. The Solubility dataset is composed of real-world molecules with different levels of solubility, where nodes and edges represent atoms and their chemical bonds, respectively. In our experiments, we ignore the edge connection types. Although this dataset was originally intended to be used as a regression task, it is partitioned into two classes for the graph classification task. We label molecules with log solubility values lower than -4 as 0, and those with values higher than -2 as 1. Rigid carbon structures are considered as the ground truth explanation for insolubility, while *R-OH* chemical groups are treated as the ground truth explanation for solubility [5], [40]. The one-hot encoded feature vector of each node represents types of atoms, which can be one of Carbon, Nitrogen, Oxygen, Fluorine, Iodine, Chlorine, Phosphorus, Sulfur, Hydrogen, and Bromine.

Note that model-level explanation methods aim to discover explanations depending on the classes of each dataset. Thus, in all the experiments, model-level explanation methods use the class including a precise subgraph pattern as input and then attempt to retrieve the class-distinctive subgraph as the prototype graph.

5.2 Benchmark Method

In this subsection, we present a state-of-the-art method for comparison. To the best of our knowledge, XGNN [17] is the sole model-level explanation method for GNNs, which trains a graph generator that generates a subgraph pattern (i.e., a prototype graph) via reinforcement learning in the sense of maximizing a certain prediction of the underlying GNN model.

It is worth noting that there have been earlier studies on model-level explanations for CNNs based on input optimization using computer vision datasets [26], [27], [28]. However, extending these approaches to graph domains faces non-trivial technical challenges. This is because, the application of input optimization methods into GNNs can be viewed as synthesizing both a graph pattern (i.e., an adjacency matrix) and node features in the sense of maximizing the output probabilities of the target GNN for certain classes, which is computationally expensive and needs to consider the sparse nature of graphs. Thus, instead of such an extension, as an alternative, we shall study the relationship between PAGE and instance-level GNN explanation methods in Section 5.4.4.

5.3 Experimental Settings

We first describe the settings of the GNN model. We adopt GCN [29] as one of the widely used GNN architectures. The summation function is used as a readout function. We use 2 GNN layers for the BA-house and BA-grid datasets and 3 GNN layers for other three datasets unless otherwise stated. We set the dimension of each hidden latent space to 32 for all the datasets. We train the GNN model with Adam optimizer [41] with a learning rate of 0.001 and a batch size of 16. For all five datasets, we split each dataset into training/validation/test sets with a ratio of 90/5/5%. The training set is used to learn the model parameters with

the cross-entropy loss; and the validation set is used for early stopping with a patience of 5 epochs. We report the graph classification performance on the test set along with the datasets in Table 2.

Next, we turn to describing the settings of explanation methods including PAGE and XGNN. In PAGE, the implementations of clustering with the GMM are those from the scikit-learn Python package [42]. We set $L = 2$ and $k = 3$ used in Phase 1. We also set *budget*, indicating the number of search sessions, to 5. Additionally, we set the decay rate and the maximum number of iterations used in the iterative subgraph search (Step 2 of Phase 2) as 10 and 1,000, respectively. For the implementations of XGNN, we tuned the hyperparameters by essentially following the same settings as those in the original paper [17].

The GNN model and explanation methods used in our experiments were implemented with Python 3.8.12, PyTorch 1.11.0, PyTorch Geometric 2.0.4 [43], and Captum 0.5.0 [44], and were run on a machine with an Intel Core i7-9700K 3.60 GHz CPU with 32GB RAM and a single NVIDIA GeForce RTX 3080 GPU.

5.4 Experimental Results

Our experiments are designed to answer the following five key research questions (RQs).

- **RQ1:** How are the model-level explanations of PAGE *qualitatively* evaluated in comparison with the benchmark method?
- **RQ2:** How are the model-level explanations of PAGE *quantitatively* evaluated in comparison with the benchmark method?
- **RQ3:** When does PAGE return the final prototype graph during multiple search sessions?
- **RQ4:** How do the explanations of PAGE relate to instance-level explanation methods?
- **RQ5:** How many input graphs does PAGE require for model-level explanations?
- **RQ6:** How effective is the prototype scoring function in PAGE in comparison with naïve alternatives?

5.4.1 Qualitative Analysis of Model-Level Explanation Methods (RQ1)

We perform a qualitative evaluation of both PAGE and XGNN by visualizing their explanations (i.e., prototype graphs) along with the ground truth explanations for each dataset. As illustrated in Fig. 5, we observe that the explanations discovered by PAGE and the ground truth explanations exhibit a high similarity in terms of the graph structure and node features (i.e., types of nodes), while XGNN mostly fails to produce prototypes that contain the entire ground truth explanations. From Fig. 5, our findings for each dataset are as follows:

- For the BA-house dataset, PAGE successfully returns the class-discriminative subgraphs that we add to the backbone graph, that is, the house-shaped subgraphs on BA-house. However, the prototypes generated by XGNN contain only parts of the house-shaped subgraphs. For instance, the outcome from XGNN

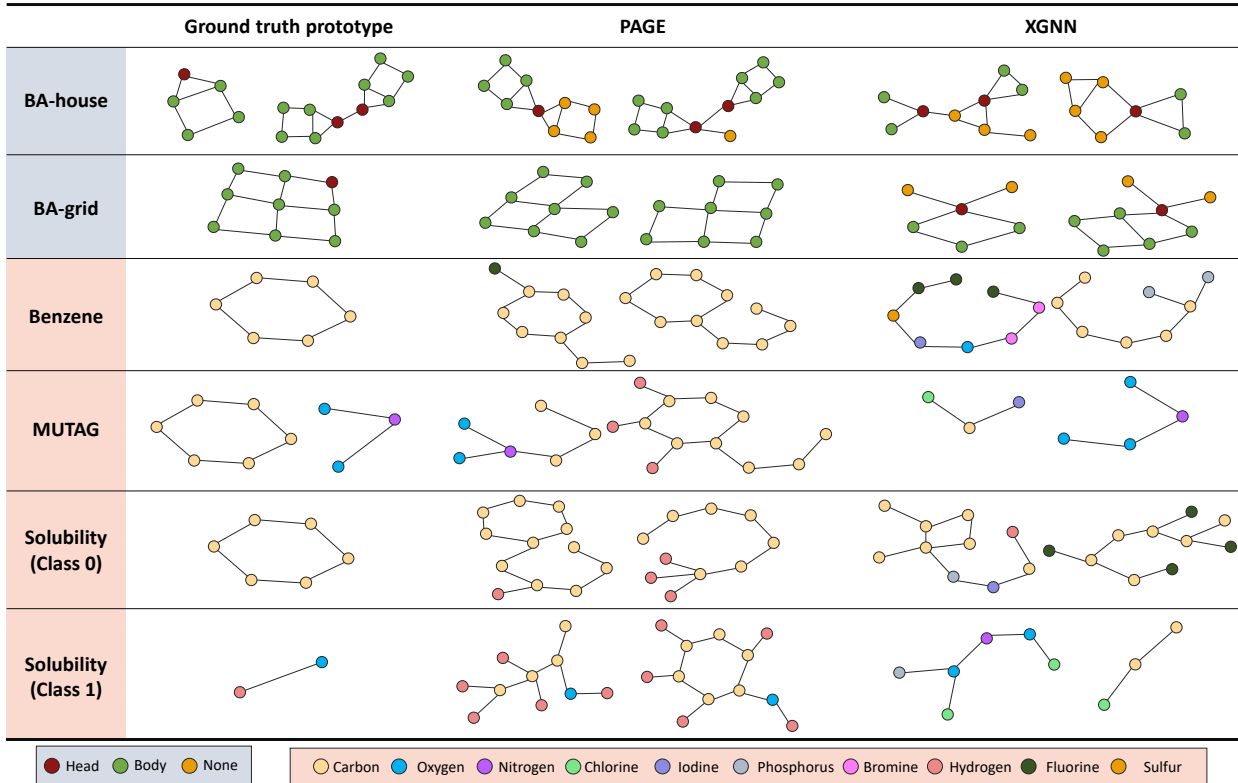


Fig. 5: Qualitative comparison of PAGE and XGNN for five datasets, where each node is colored differently according to the types of nodes.

contains only three out of five nodes of the house-shaped subgraph, thus making the explanation incomplete. On the other hand, PAGE can produce much more precise explanations by returning two types of prototype graphs containing either a single or double house-shaped subgraph. Such preciseness of PAGE is possible primarily due to the usage of clustering of graph-level embeddings.

- The results from the BA-grid dataset show a tendency similar to those on BA-house. PAGE returns most of grid-like subgraphs, while XGNN recovers smaller portions of them.
- For the case of the Benzene dataset, PAGE correctly identifies the ring structure with 6 carbon atoms as a part of the prototype graph, while XGNN does not generate any carbon ring. Although XGNN produces six carbon atoms, it fails to connect the atoms to a closed ring structure.
- For the MUTAG dataset having two types of prototype graphs, PAGE identifies both carbon rings and NO_2 chemical groups. However, XGNN only recovers NO_2 while generating small molecules.
- We analyze model-level explanations for two classes on Solubility. For Class 0 (i.e., the case classified as insoluble molecules), PAGE tends to return carbon atoms and occasionally adds hydrogen atoms; XGNN also produces prototypes with mostly carbon atoms but contains a large portion of non-carbon atoms. Unlike the case of PAGE, XGNN fails to produce the carbon ring structure. For Class 1 (i.e.,

the case classified as soluble molecules), PAGE correctly identifies the $R-OH$ chemical group for all prototypes; in contrast, XGNN fails to include $R-OH$ for its explanations.

5.4.2 Quantitative Analysis of Model-Level Explanation Methods (RQ2)

For the quantitative analysis, we adopt two performance metrics from [19]: *consistency* and *faithfulness*. Although they were originally designed for evaluating the performance of instance-level GNN explanation methods, they are extended to model-level GNN explanation methods with modifications in such a way that the output probability for the explanation is taken into account as a proxy for measuring the superiority of the resulting explanation. We first describe the two metrics used for evaluation.

- **Consistency** measures the robustness of explanations for different settings of GNN models. Since the task (i.e., graph classification) does not change in each experiment, reliable explanation methods should produce *stable* explanations despite different model configurations. In our experiments for model-level explanations, we calculate the *standard deviation* of output probabilities for the explanations (e.g., the prototype graphs retrieved by PAGE) across different GNN hyperparameter settings. To this end, we generate multiple GNN models with various combinations of the hidden layer dimension. For the BA-house and BA-grid datasets, we produce 25 models with $\{4, 8, 16, 32, 64\} \times \{4, 8, 16, 32, 64\}$ hidden di-

Method	BA-house	BA-grid	Solubility	MUTAG	Benzene
PAGE	0.0308	0.0615	0.0846	0.1216	0.0639
XGNN	0.2152	0.2705	0.3213	0.1269	0.2227

(a) Consistency.

Method	BA-house	BA-grid	Solubility	MUTAG	Benzene
PAGE	0.7340	0.5636	0.2164	0.4430	0.2364
XGNN	-0.4037	-0.1636	0.0983	0.2504	-0.3091

(b) Faithfulness.

TABLE 3: Quantitative assessment results for PAGE and XGNN with respect to the consistency (the lower the better) and faithfulness (the higher the better) for five datasets.

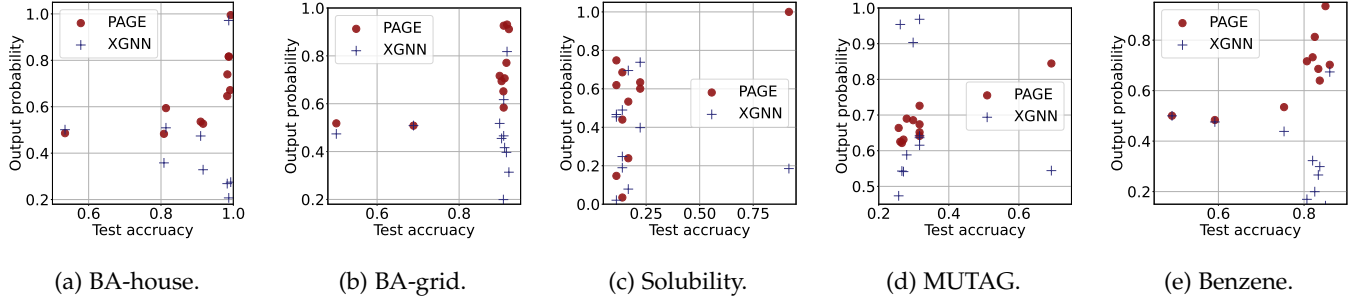


Fig. 6: Visualization of the output probabilities of explanations versus the GNN’s test accuracies for measuring the faithfulness when PAGE and XGNN are used as model-level explanation methods.

mension configurations. For the Benzene, Solubility, and MUTAG datasets, we produce 64 models with $\{4, 8, 16, 32\} \times \{4, 8, 16, 32\} \times \{4, 8, 16, 32\}$ hidden dimension configurations. The lower the value of consistency, the better the performance.

- **Faithfulness** measures how closely the explanation method reflects the GNN model’s behavior. Following [19], we regard the test accuracy of the model as the behavior of interest, and empirically observe the relationship between the output probabilities of explanations and the GNN’s test accuracies. An ideal explanation method will not only produce explanations with high output probabilities when the model is sufficiently trained, but also return undesirable explanations when the model does not perform appropriately. In our experiments, faithfulness is measured by the Kendall’s tau coefficient [45] between the output probability p_{GNN} for the explanation and the GNN’s test accuracy (i.e., the performance on graph classification), which represents the degree to which the explanations reflect the GNN’s test accuracies. To this end, we acquire a set of GNN models leading to varying accuracies by corrupting portions of labels in the training set from 0% to 50% in increment of 5%. The higher the value of faithfulness, the better the performance.

Table 3 summarizes quantitative evaluations for PAGE and XGNN with respect to the consistency and faithfulness when five datasets are used. In Table 3a, we observe that PAGE provides more stable explanations across different hidden dimension configurations than those of XGNN for all datasets; from Table 3b, we observe that PAGE apparently exhibits a positive correlation between the GNN’s test accuracies and the output probabilities compared to XGNN, which implies that PAGE is able to successfully account for what the GNN model has learned about its explanation outcome.

To further analyze the faithfulness for PAGE and XGNN, we visualize scatter plots of the output probabilities of explanations versus the GNN’s test accuracies in Fig. 6. The intriguing observations are made from Table 3b and Fig. 6:

- The different tendency between PAGE and XGNN is apparent on BA-house, BA-grid, and Benzene. For the Solubility and MUTAG datasets, the GNN’s test accuracy tends to be quite low when labels are corrupted, which thus does not exhibit a clear relationship between the output probability and the test accuracy. This implies that the two datasets are more challenging to be learned in such noisy settings.
- Overall, the performance difference PAGE and XGNN in terms of the faithfulness becomes more prominent for the synthetic datasets. This is because the ground truth explanation can establish a relationship with the corresponding class more clearly due to less noise of the synthetic datasets.
- XGNN reveals a negative Kendall’s tau coefficient for some datasets.
- This is because, when the GNN model is trained with high label corruption ratios, it basically passes through as a random classifier and thus cannot decide whether the explanation generated from XGNN is valid or not. When the GNN model is trained with fewer corrupted data, it now learns the characteristics of the given dataset and will produce low output probabilities if the outcome of XGNN does not contain the complete ground truth prototype. Eventually, this results in a negative correlation between the output probability versus the GNN’s test accuracy.

5.4.3 Impact of Multiple Search Sessions in PAGE (RQ3)

Aside from the final prototype graph of PAGE, we are also interested in analyzing the output probability p_{GNN} calculated for each search session in order to see when the

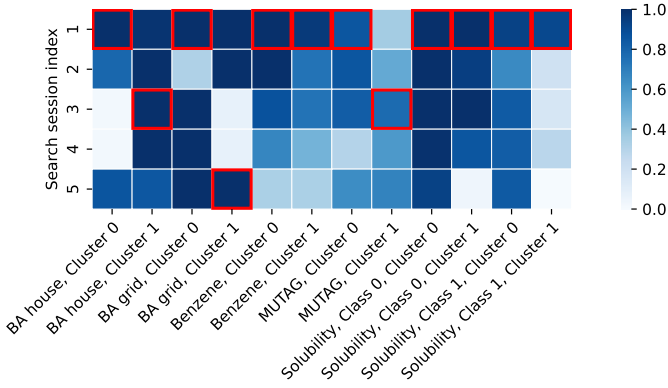


Fig. 7: Heatmap visualization of the output probability for the discovered subgraph in each search session when PAGE is used for all datasets. The subgraph returned as the final prototype graph is marked with a red box.

prototype candidate having the highest p_{GNN} is selected over *budget* search sessions. Fig. 7 visualizes a heatmap of the output probability p_{GNN} for the discovered subgraph (i.e., the prototype candidate) in each session for all datasets, being partitioned into two clusters for a certain class, when *budget* is given by 5. The prototype candidate chosen as the final prototype graph $g_l^{(c)}$ is highlighted with a red box for each case. We would like to make the following observations:

- In most cases, each search session tends to return a prototype candidate with various values of p_{GNN} . For example, in Cluster 1 of MUTAG, the resultant p_{GNN} 's of the discovered prototype candidates range from the values near 0.4 to the ones near 0.8, which faithfully reflects our intention for the design of the core prototype search module (see Section 4.2.2).
- The first search session produces the final explanation (i.e., the final prototype graph $g_l^{(c)}$) for 7 out of 10 cases. This tendency is expected since the first search session starts the iterative subgraph search (Step 2 of Phase 2 in Section 4.2.3) alongside the highest matching score in \mathbf{Y}_l .
- There are a few cases in which the prototype candidate returned by a search session other than the first one is chosen as the final prototype graph, thereby justifying the necessity of multiple search sessions.
- From these observations, one can see that the number of search sessions, namely *budget*, will not be a critical problem in determining the performance of PAGE.

5.4.4 Relation Between PAGE and Instance-Level Explanations (RQ4)

Since most studies on GNN explanations focus on developing instance-level explanation methods, we perform an additional analysis by investigating the relationship between our proposed PAGE method and instance-level explanation methods. Specifically, after discovering the prototype graph $g_l^{(c)}$ along with PAGE, we use $g_l^{(c)}$ as input to an instance-level explanation method to acquire the attribution map (also known as the saliency map). That is, we are interested in evaluating attribution for each node in $g_l^{(c)}$, which

indicates its significance towards making the model decisions. This evaluation can be interpreted as measuring the agreement between PAGE and instance-level explanation methods.

For a graph $G_i = (\mathcal{V}_i, \mathcal{E}_i, \mathcal{X}_i)$, an instance-level explanation method takes a node v in a graph as input and returns its attribution score, denoted as $\Lambda(v)$, which is normalized across all nodes in the graph. We present the following two quantities that we define in our experiments.

Definition 2 (Concentration score). Given a prototype graph $g_l^{(c)}$ and the ground truth explanation $g_T^{(c)}$, we define the *concentration score* α as follows:

$$\alpha = \sum_{v \in \mathcal{V}_{g_T^{(c)}} \cap \mathcal{V}_{g_l^{(c)}}} \Lambda(v), \quad (12)$$

where $\mathcal{V}_{g_T^{(c)}}$ and $\mathcal{V}_{g_l^{(c)}}$ are the sets of nodes belonging to subgraphs $g_T^{(c)}$ and $g_l^{(c)}$, respectively. The concentration score measures how much the instance-level explanation concentrates on the nodes belonging to the ground truth explanation $g_T^{(c)}$. If none of the nodes in the prototype $g_l^{(c)}$ belongs to $g_T^{(c)}$, then α becomes zero. The higher the value of α lying between 0 and 1, the better the performance.

Definition 3 (Relative training gain). Given the concentration score α for a prototype graph $g_l^{(c)}$ and the ground truth explanation $g_T^{(c)}$, the *relative training gain* β is defined as

$$\beta = \frac{\alpha}{\alpha_0} - 1, \quad (13)$$

where α_0 denotes the concentration score calculated using an initialized GNN model before training for the same prototype graph $g_l^{(c)}$.

The relative training gain measures the relative gain of the concentration score after the GNN model has been trained. The higher the value of β , the better the performance. Note that β differs from the faithfulness in that it focuses on the *relationship* between model-level and instance-level explanation methods.

In our experiments, we adopt the following two instance-level explanation methods:

- **Input \times Gradient** [46]: This method takes the gradients of the output with respect to the input and multiplies by the input in order to produce attribution maps.
- **GNNExplainer** [6]: Given an input instance, this method identifies a subgraph structure and a small subset of node features that are most influential to GNN's prediction. GNNExplainer performs an optimization task in the sense of maximizing the mutual information between the prediction and the distribution of possible subgraph structures.

Table 4 summarizes quantitative evaluations for measuring the agreement between PAGE and two instance-level explanation methods with respect to the concentration score α and the relative training gain β when the BA-house and Benzene datasets (i.e., one synthetic dataset and one real-world dataset) are used. To further analyze the relation between PAGE and two instance-level explanation methods,

Method	α	β
Input \times Gradient	0.9128	1.5919
GNNExplainer	0.8458	0.0477

(a) BA-house.

Method	α	β
Input \times Gradient	0.4193	-0.0592
GNNExplainer	0.7028	0.0170

(b) Benzene.

TABLE 4: Quantitative assessment results of measuring the agreement between PAGE and two instance-level explanation methods for the BA-house and Benzene datasets.

we visualize the attribution score as a heatmap where the two instance-level explanation methods are adopted to the output prototype graphs discovered by PAGE for the two datasets in Fig. 8.

We first analyze the quantitative assessment results with respect to α in Table 4 and Fig. 8.

- For the BA-house dataset, the values of α achieved by both Input \times Gradient and GNNExplainer are sufficiently high, which indicates that a vast majority of attribution scores are assigned to the nodes belonging to the house-shaped subgraphs. In other words, the performance of PAGE and two instance-level explanation methods is shown to behave closely and consistently with each other.
- For the Benzene dataset, although the above tendency is observed similarly for GNNExplainer, the value of α tends to diminish for Input \times Gradient. It is known that gradient-based attribution methods may often fail to capture the GNN model’s behavior since activation functions such as Rectified Linear Units (ReLU) have a gradient of zero when they are not activated during the feed-forward process of GNN [46].

We turn to analyzing the quantitative assessment results with respect to β in Table 4.

- One can expect to see a positive value of β if the performance of both PAGE and instance-level explanation methods behaves closely and consistently.
- However, a negative value of β is observed for the case of Input \times Gradient on Benzene, which is in contrast to the case of GNNExplainer producing positive values of β for the two datasets.
- The higher agreement between PAGE and GNNExplainer is due to the fact that GNNExplainer was designed for generating explanations on graphs and GNN models, thus reliably producing the resulting attributions.

Note that the results from other three datasets showed a tendency similar to those reported in Section 5.4.4.

5.4.5 Robustness to the Number of Available Input Graphs (RQ5)

We now perform a qualitative evaluation of PAGE by visualizing the resultant prototype graphs in a more difficult

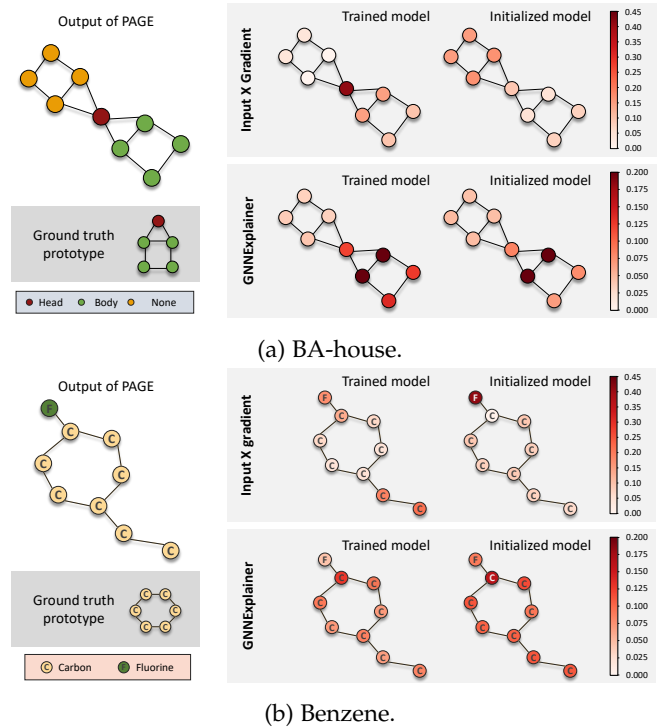


Fig. 8: Visualization of the attribution score as a heatmap where Input \times Gradient and GNNExplainer are adopted to the output prototype graphs from PAGE for the BA-house and Benzene datasets.

setting where each dataset is composed of only a few available graphs $\tilde{\mathcal{G}} \subset \mathcal{G}$ as input of PAGE. This often occurs in real environments since users and organizations aiming at designing explanation methods may have limited access to the input data. To emulate such a scenario, we create the subset $\tilde{\mathcal{G}}$ via random sampling from \mathcal{G} . In other words, the subset $\tilde{\mathcal{G}}$ is used for running PAGE while the GNN model has been trained using \mathcal{G} . Due to the fact that clustering of graph-level embeddings in Phase 2 of PAGE is not possible alongside only a few graphs in $\tilde{\mathcal{G}}$, we simplify PAGE and perform Phase 2 only after selecting k graphs from $\tilde{\mathcal{G}}$ instead of the k NNs.

Fig. 9 visualizes the prototype graphs discovered by simplified PAGE for five independent trials when the subset $\tilde{\mathcal{G}}$ of the BA-house and Benzene datasets is used for $k = 3$. In the case of BA-house in Fig. 9a, we observe that the prototype contains an entire single house-shaped subgraph for four out of five trials, indicating that the core prototype search module is capable of producing ground truth explanations even in the incomplete dataset setting. However, due to the absence of clustering, the prototype graph containing double house-shaped subgraphs is not retrieved. Therefore, the simplified PAGE does not produce precise explanations but resorts to simpler explanations. In the case of Benzene in Fig. 9b, we observe that the carbon ring structure is included for all five trials; the number of atoms other than the ground truth explanation varies over different trials due to the random selection of graph subsets $\tilde{\mathcal{G}}$. Note that the results from other three datasets also follow similar trends although not shown in the manuscript.

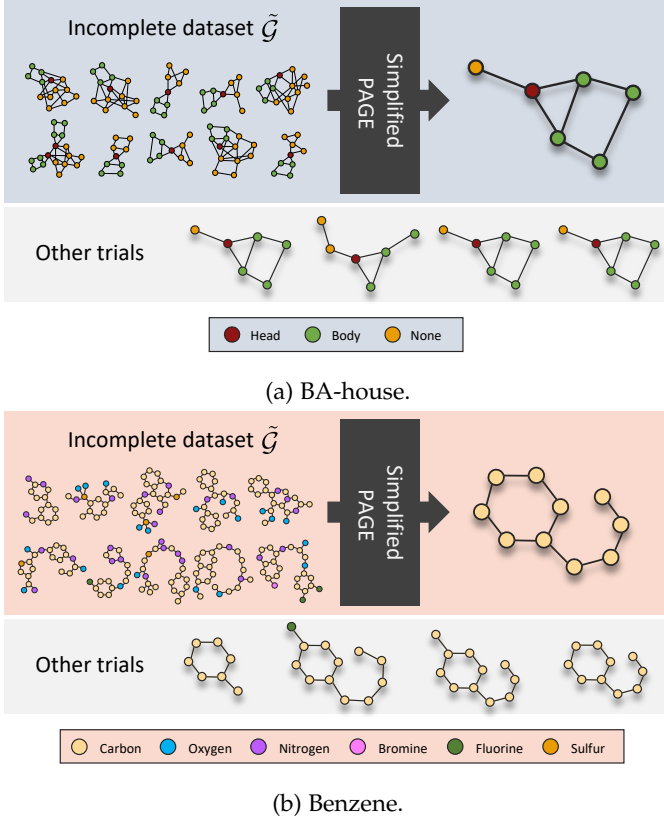


Fig. 9: Qualitative analysis of PAGE in an incomplete dataset setting, where each node is colored differently according to the types of nodes.

5.4.6 Effectiveness of the Prototype Scoring Function (RQ6)

We validate the effectiveness of our prototype scoring function s in Definition 1 in terms of the computation efficiency in comparison to a naïve alternative. Instead of acquiring a set of node-level embedding vectors through a certain GNN model, we synthetically generate and feed them into the function s , which is sufficient to analyze the effectiveness of s . Specifically, we first generate each Gaussian random vector \mathbf{w}_i with zero mean and covariance matrix \mathbf{I}_b , i.e., $\mathbf{w}_i \sim \mathcal{N}(\mathbf{0}_b, \mathbf{I}_b)$, where $\mathbf{0}_b$ and \mathbf{I}_b denote the zero vector and the identity matrix, respectively, of size b . Then, the vectors \mathbf{w}_i 's pass through the ReLU activation function $\mathbf{v}_i = \text{ReLU}(\mathbf{w}_i)$, which corresponds to a synthetic node-level embedding vector.

In our experiments, we generate 10^3 3-tuples of vectors, which are used as the input of $s(\mathbf{v}_1, \mathbf{v}_2, \mathbf{v}_3)$. We compare s with the following alternative prototype scoring functions: $s_{AM}(\mathbf{v}_1, \mathbf{v}_2, \mathbf{v}_3) = (\mathbf{v}_1^T \mathbf{v}_2 + \mathbf{v}_2^T \mathbf{v}_3 + \mathbf{v}_3^T \mathbf{v}_1)/3$ and $s_{GM}(\mathbf{v}_1, \mathbf{v}_2, \mathbf{v}_3) = (\mathbf{v}_1^T \mathbf{v}_2 \times \mathbf{v}_2^T \mathbf{v}_3 \times \mathbf{v}_3^T \mathbf{v}_1)^{1/3}$, which return the arithmetic mean and the geometric mean, respectively, of all possible inner products between pairs of embedding vectors.

We empirically show the average runtime complexities of s , s_{AM} , and s_{GM} in Table 5. This experiment reveals that s_{AM} and s_{GM} are more computationally expensive than s , which is consistent with our analysis in Remark 1. Additionally, Fig. 10 visualizes scatter plots of the proposed s

Prototype scoring function	s	s'_{AM}	s'_{GM}
Time (μs)	14.42 ± 12.65	38.34 ± 17.81	31.39 ± 17.81

TABLE 5: Comparison of different prototype scoring functions in terms of the runtime complexity in microseconds (mean \pm standard deviation).

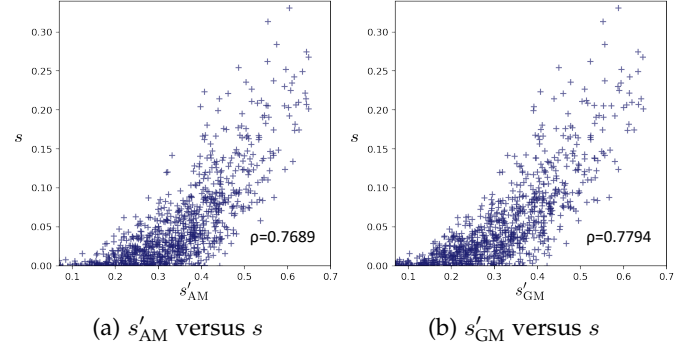


Fig. 10: Visualization of the results of different prototype scoring functions along with the correlation coefficient ρ .

versus each of the naïve alternative, i.e., either s_{AM} or s_{GM} . From this figure, we observe a high correlation between two, where the Pearson correlation coefficient ρ is more than 0.75 for both cases. This demonstrates that our prototype scoring function s is a good approximation of the calculation of all possible inner products between embedding pairs.

6 CONCLUSIONS AND OUTLOOK

We investigated a largely underexplored yet important problem of explaining the decisions of GNNs at the model level. To tackle this practical challenge, we introduced a novel explanation method that offers model-level explanations of GNNs for the graph classification task by discovering prototypes from both node-level and graph-level embeddings. Specifically, we designed PAGE, an effective two-phase model-level GNN explanation method; after performing clustering and selection of graph-level embeddings in Phase 1, we perform prototype discovery in Phase 2, which is partitioned into the initialization, iterative sub-graph search, and prototype retrieval steps. Furthermore, we theoretically validated the usage of clustering of graph-level embeddings in PAGE. Using two synthetic and three real-world datasets, we comprehensively demonstrated that PAGE is superior to the state-of-the-art model-level GNN explanation method both qualitatively and quantitatively. Additionally, through systematic evaluations, we proved the effectiveness of PAGE in terms of 1) the impact of multiple search sessions in the core prototype search module, 2) the relation to instance-level explanation methods via quantitative assessment, 3) the robustness to a difficult and challenging situation where only a few graphs are available as input of PAGE, and 4) the computational efficiency of the proposed prototype scoring function.

Potential avenues of future research include the design of model-level GNN explanation methods for the node-level or edge-level classification task.

ACKNOWLEDGMENTS

This research was supported by the National Research Foundation of Korea (NRF) grant funded by the Korea government (MSIT) (No. 2021R1A2C3004345). The material in this paper was presented in part at the AAAI Conference on Artificial Intelligence, Virtual Event, February/March 2022 [47].

REFERENCES

- [1] Z. Wu, S. Pan, F. Chen, G. Long, C. Zhang, and P. S. Yu, "A comprehensive survey on graph neural networks," *IEEE Trans. Neural Netw. Learn. Syst.*, vol. 32, no. 1, pp. 4–24, Jan. 2021.
- [2] K. Xu, W. Hu, J. Leskovec, and S. Jegelka, "How powerful are graph neural networks?" in *Proc. 7th Int. Conf. Learn. Representations (ICLR'19)*, New Orleans, LA, May 2019.
- [3] W. Samek and K. Müller, "Towards explainable artificial intelligence," in *Explainable AI: Interpreting, Explaining and Visualizing Deep Learning*, 1st ed., ser. Lecture Notes in Computer Science, W. Samek, G. Montavon, A. Vedaldi, L. K. Hansen, and K. Müller, Eds. Cham, Switzerland: Springer, 2019, vol. 11700, pp. 5–22.
- [4] M. T. Ribeiro, S. Singh, and C. Guestrin, "Why should I trust you?: Explaining the predictions of any classifier," in *Proc. 22nd ACM SIGKDD Int. Conf. Knowl. Discovery & Data Mining (KDD'16)*, San Francisco, CA, Aug. 2016, pp. 1135–1144.
- [5] F. Baldassarre and H. Azizpour, "Explainability techniques for graph convolutional networks," in *Proc. ICML Workshop on Learning and Reasoning with Graph-Structured Data*, Long Beach, CA, Jun. 2019.
- [6] Z. Ying, D. Bourgeois, J. You, M. Zitnik, and J. Leskovec, "GN-NEExplainer: Generating explanations for graph neural networks," in *Proc. 30th Int. Conf. Neural Inf. Process. Syst. (NeurIPS'19)*, Vancouver, Canada, Dec. 2019.
- [7] L. Faber, A. K. Moghaddam, and R. Wattenhofer, "Contrastive graph neural network explanation," in *ICML Workshop on Graph Representation Learning and Beyond*, Virtual Event, Jul. 2020.
- [8] H. Yuan, H. Yu, J. Wang, K. Li, and S. Ji, "On explainability of graph neural networks via subgraph explorations," in *Proc. 38th Int. Conf. Mach. Learn. (ICML'21)*, vol. 139, Virtual Event, Jul. 2021, pp. 12 241–12 252.
- [9] D. Luo, W. Cheng, D. Xu, W. Yu, B. Zong, H. Chen, and X. Zhang, "Parameterized explainer for graph neural network," in *Proc. 31st Int. Conf. Neural Inf. Process. Syst. (NeurIPS'20)*, Virtual Event, Dec. 2020.
- [10] M. S. Schlichtkrull, N. D. Cao, and I. Titov, "Interpreting graph neural networks for NLP with differentiable edge masking," in *Proc. 9th Int. Conf. Learn. Representations (ICLR'21)*, Virtual Event, May 2021.
- [11] T. Schnake, O. Eberle, J. Lederer, S. Nakajima, K. T. Schutt, K. Mueller, and G. Montavon, "Higher-order explanations of graph neural networks via relevant walks," *IEEE Trans. Pattern Anal. Mach. Intell.*, vol. 44, no. 11, pp. 7581–7596, 2022.
- [12] W. Lin, H. Lan, and B. Li, "Generative causal explanations for graph neural networks," in *Proc. 38th Int. Conf. Mach. Learn. (ICML'21)*, Virtual Event, Jul. 2021, pp. 6666–6679.
- [13] M. N. Vu and M. T. Thai, "PGM-Explainer: Probabilistic graphical model explanations for graph neural networks," in *Proc. 31st Int. Conf. Neural Inf. Process. Syst. (NeurIPS'20)*, Virtual Event, Dec. 2020.
- [14] A. Lucic, M. A. ter Hoeve, G. Tolomei, M. de Rijke, and F. Silvestri, "CF-GNNExplainer: Counterfactual explanations for graph neural networks," in *Proc. 25th Int. Conf. Artif. Intell. Statist. (AISTATS'22)*, vol. 151, Virtual Event, Mar. 2022, pp. 4499–4511.
- [15] X. Wang, Y. Wu, A. Zhang, F. Feng, X. He, and T. Chua, "Reinforced causal explainer for graph neural networks," *IEEE Trans. Pattern Anal. Mach. Intell.*, vol. Early access, pp. 1–12, 2022.
- [16] H. Yuan, H. Yu, S. Gui, and S. Ji, "Explainability in graph neural networks: A taxonomic survey," *IEEE Trans. Pattern Anal. Mach. Intell.*, vol. Early access, pp. 1–19, 2022.
- [17] H. Yuan, J. Tang, X. Hu, and S. Ji, "XGNN: Towards model-level explanations of graph neural networks," in *Proc. 26th ACM SIGKDD Int. Conf. Knowl. Discovery & Data Mining (KDD'20)*, Virtual Event, Aug. 2020, pp. 430–438.
- [18] C. Yang, A. Rangarajan, and S. Ranka, "Global model interpretation via recursive partitioning," in *IEEE 20th International Conference on High Performance Computing and Communications; IEEE 16th International Conference on Smart City; IEEE 4th International Conference on Data Science and Systems (HPCC/SmartCity/DSS'18)*, Exeter, UK, Jun. 2018, pp. 1563–1570.
- [19] B. Sanchez-Lengeling, J. N. Wei, B. K. Lee, E. Reif, P. Wang, W. W. Qian, K. McCloskey, L. J. Colwell, and A. B. Wiltchko, "Evaluating attribution for graph neural networks," in *Proc. 31st Int. Conf. Neural Inf. Process. Syst. (NeurIPS'20)*, Virtual Event, Dec. 2020.
- [20] G. Montavon, W. Samek, and K.-R. Müller, "Methods for interpreting and understanding deep neural networks," *Digit. Signal Process.*, vol. 73, pp. 1–15, 2018.
- [21] J. T. Springenberg, A. Dosovitskiy, T. Brox, and M. A. Riedmiller, "Striving for simplicity: The all convolutional net," in *Proc. 3rd Int. Conf. Learn. Representations (ICLR'15), Workshop Track Proceedings*, San Diego, CA, May 2015.
- [22] S. Bach, A. Binder, G. Montavon, F. Klauschen, K.-R. Müller, and W. Samek, "On pixel-wise explanations for non-linear classifier decisions by layer-wise relevance propagation," *PloS One*, vol. 10, no. 7, p. e0130140, 2015.
- [23] G. Montavon, A. Binder, S. Lapuschkin, W. Samek, and K. Müller, "Layer-wise relevance propagation: An overview," in *Explainable AI: Interpreting, Explaining and Visualizing Deep Learning*, ser. Lecture Notes in Computer Science, W. Samek, G. Montavon, A. Vedaldi, L. K. Hansen, and K. Müller, Eds. Cham, Switzerland: Springer, 2019, vol. 11700, pp. 193–209.
- [24] M. Sundararajan, A. Taly, and Q. Yan, "Axiomatic attribution for deep networks," in *Proc. 34th Int. Conf. Mach. Learn. (ICML'17)*, Sydney, Australia, Aug. 2017, pp. 3319–3328.
- [25] R. R. Selvaraju, M. Cogswell, A. Das, R. Vedantam, D. Parikh, and D. Batra, "Grad-CAM: Visual explanations from deep networks via gradient-based localization," in *Proc. IEEE Int. Conf. Comput. Vision, (ICCV'17)*, Venice, Italy, Oct. 2017, pp. 618–626.
- [26] A. M. Nguyen, J. Yosinski, and J. Clune, "Deep neural networks are easily fooled: High confidence predictions for unrecognizable images," in *Proc. IEEE Conf. Comput. Vision Pattern Recognit. (CVPR'15)*, Boston, MA, Jun. 2015, pp. 427–436.
- [27] A. M. Nguyen, A. Dosovitskiy, J. Yosinski, T. Brox, and J. Clune, "Synthesizing the preferred inputs for neurons in neural networks via deep generator networks," in *Proc. 27th Int. Conf. Neural Inf. Process. Syst. (NeurIPS'16)*, Barcelona, Spain, Dec. 2016, pp. 3387–3395.
- [28] A. Nguyen, J. Clune, Y. Bengio, A. Dosovitskiy, and J. Yosinski, "Plug & play generative networks: Conditional iterative generation of images in latent space," in *Proc. IEEE Conf. Comput. Vision Pattern Recognit. (CVPR'17)*, Honolulu, HI, Jul. 2017, pp. 3510–3520.
- [29] T. N. Kipf and M. Welling, "Semi-supervised classification with graph convolutional networks," in *Proc. 5th Int. Conf. Learn. Representations (ICLR'17)*, Toulon, France, 2017.
- [30] C. W. J. Granger, "Investigating causal relations by econometric models and cross-spectral methods," *Econometrica*, vol. 37, no. 3, pp. 424–438, 1969.
- [31] J. Gilmer, S. S. Schoenholz, P. F. Riley, O. Vinyals, and G. E. Dahl, "Neural message passing for quantum chemistry," in *Proc. 34th Int. Conf. Mach. Learn. (ICML'17)*, vol. 70, Sydney, Australia, Aug. 2017, pp. 1263–1272.
- [32] C. M. Bishop, *Pattern Recognition and Machine Learning (Information Science and Statistics)*, 2nd ed. New York, NY: Springer, 2006.
- [33] A. P. Dempster, N. M. Laird, and D. B. Rubin, "Maximum likelihood from incomplete data via the em algorithm," *J. Royal Stat. Soc. Series B (Methodological)*, vol. 39, no. 1, pp. 1–38, 1977.
- [34] N. Shervashidze, P. Schweitzer, E. J. van Leeuwen, K. M. Mehlhorn, and K. M. Borgwardt, "Weisfeiler-Lehman graph kernels," *J. Mach. Learn. Res.*, vol. 12, pp. 2539–2561, 2011.
- [35] V. Arvind, J. Köbler, G. Rattan, and O. Verbitsky, "On the power of color refinement," in *Proc. Fundam. Comput. Theory - 20th Int. Symp. (FCT 2015)*, ser. Lecture Notes in Computer Science, vol. 9210, Gdańsk, Poland, Aug. 2015, pp. 339–350.
- [36] C. Morris, M. Ritzert, M. Fey, W. L. Hamilton, J. E. Lenssen, G. Rattan, and M. Grohe, "Weisfeiler and leman go neural: Higher-order graph neural networks," in *Proc. 33rd AAAI Conf. Artif. Intell. (AAAI'19)*, Honolulu, HI, Jan.-Feb. 2019, pp. 4602–4609.
- [37] L. van der Maaten and G. Hinton, "Visualizing data using t-SNE," *J. Mach. Learn. Res.*, vol. 9, no. 86, pp. 2579–2605, 2008.

- [38] K. McCloskey, A. Taly, F. Monti, M. P. Brenner, and L. J. Colwell, "Using attribution to decode binding mechanism in neural network models for chemistry," *Proc. Nat. Acad. Sci.*, vol. 115, no. 23, pp. 11 623–11 629, 2018.
- [39] A. K. Debnath, R. L. Lopez de Compadre, G. Debnath, A. J. Shusterman, and C. Hansch, "Structure-activity relationship of mutagenic aromatic and heteroaromatic nitro compounds. Correlation with molecular orbital energies and hydrophobicity," *J. Med. Chem.*, vol. 34, no. 2, pp. 786–797, Feb 1991.
- [40] D. Duvenaud, D. Maclaurin, J. Aguilera-Iparraguirre, R. Gómez-Bombarelli, T. Hirzel, A. Aspuru-Guzik, and R. P. Adams, "Convolutional networks on graphs for learning molecular fingerprints," in *Proc. 26th Int. Conf. Neural Inf. Process. Syst. (NeurIPS'15)*, Montreal, Canada, Dec. 2015, pp. 2224–2232.
- [41] D. P. Kingma and J. Ba, "Adam: A method for stochastic optimization," in *Proc. 3rd Int. Conf. Learn. Representations (ICLR'15)*, San Diego, CA, May 2015.
- [42] F. Pedregosa, G. Varoquaux, A. Gramfort, V. Michel, B. Thirion, O. Grisel, M. Blondel, P. Prettenhofer, R. Weiss, V. Dubourg, J. Vanderplas, A. Passos, D. Cournapeau, M. Brucher, M. Perrot, and E. Duchesnay, "Scikit-learn: Machine learning in Python," *J. Mach. Learn. Res.*, vol. 12, pp. 2825–2830, 2011.
- [43] M. Fey and J. E. Lenssen, "Fast graph representation learning with PyTorch Geometric," in *Proc. ICLR Workshop on Representation Learning on Graphs and Manifolds*, New Orleans, LA, May 2019.
- [44] N. Kokhlikyan, V. Miglani, M. Martin, E. Wang, B. Alsallakh, J. Reynolds, A. Melnikov, N. Kliushkina, C. Araya, S. Yan, and O. Reblitz-Richardson, "Captum: A unified and generic model interpretability library for PyTorch," in *Proc. ICLR Workshop on Responsible AI*, Virtual Event, 2021.
- [45] M. G. Kendall, "A new measure of rank correlation," *Biometrika*, vol. 30, no. 1-2, pp. 81–93, 06 1938.
- [46] A. Shrikumar, P. Greenside, A. Shcherbina, and A. Kundaje, "Not just a black box: Learning important features through propagating activation differences," *arXiv preprint arXiv:1605.01713*, 2016.
- [47] Y. Shin, S. Kim, E. Yoon, and W. Shin, "Prototype-based explanations for graph neural networks (Student Abstract)," in *Proc. 36th AAAI Conf. Artif. Intell. (AAAI'22)*, Virtual Event, Feb./Mar. 2022, pp. 13 047–13 048.